STEADY MODELS FOR MAGNETIC RECONNECTION

Moira Mary Jardine

A Thesis Submitted for the Degree of PhD
at the
University of St Andrews

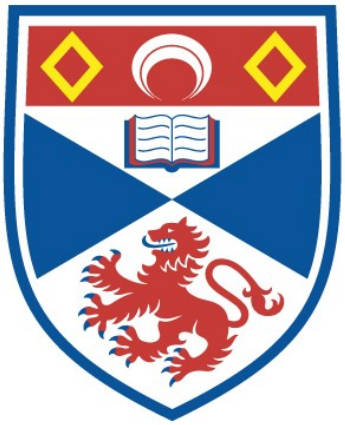

1989

Full metadata for this item is available in
St Andrews Research Repository
at:
http://research-repository.st-andrews.ac.uk/

Please use this identifier to cite or link to this item:
http://hdl.handle.net/10023/13985

This item is protected by original copyright

THE UNIVERSITY OF ST. ANDREWS

Steady models for magnetic reconnection

Moira Mary Jardine

Submitted for the degree of Ph. D.

December 1, 1988

BIBLIOTHECA UNIVERSITATIS ANDREANÆ

ProQuest Number: 10167137

All rights reserved

INFORMATION TO ALL USERS
The quality of this reproduction is dependent upon the quality of the copy submitted.

In the unlikely event that the author did not send a complete manuscript
and there are missing pages, these will be noted. Also, if material had to be removed,
a note will indicate the deletion.

ProQuest 10167137

Published by ProQuest LLC (2017). Copyright of the Dissertation is held by the Author.

All rights reserved.
This work is protected against unauthorized copying under Title 17, United States Code
Microform Edition © ProQuest LLC.

ProQuest LLC.
789 East Eisenhower Parkway
P.O. Box 1346
Ann Arbor, MI 48106 – 1346

Th A860

CONTENTS

LIST OF FIGURES

THE UNIVERSITY OF ST. ANDREWS

Steady models for magnetic reconnection

Submitted for the degree of Ph. D.

December 1, 1988

Moira Mary Jardine

ABSTRACT

Magnetic reconnection is a fundamental physical process by which stored magnetic energy may be released. It is already known that different reconnection regimes result from changes in the nature of the plasma *inflow* towards the reconnection site. In this thesis, we examine both how the *outflow* region responds to changes both in the inflow and outflow boundary conditions and also how introducing compressibility affects the results.

We find that if the inflow is *converging*, the outflow velocity is least, the width of the outflow region is greatest and the ratio of outflowing thermal to kinetic energy is greatest. Also, there is one free outflow parameter which would naturally be specified by the velocity of plasma leaving the reconnection site. We suggest that reverse currents seen in numerical simulations may result from the specification of an extra boundary condition.

In addition, we find that the main effects of including compressibility are: to enhance convergence or divergence of the inflow; to increase the maximum reconnection rate where the inflow is converging; to increase the flow speed near the reconnection site where the inflow is diverging; to give faster, narrower outflow jets; to increase variations between regimes in the energy conversion and to increase the ratio of thermal to kinetic energy in the outflow jet.

ACKNOWLEDGMENTS

There are many unsung heroes associated with any thesis. The silent mass of flatmates, officemates and friends who witness the agony and suffering involved. They rarely get mentioned anywhere else, so I would like to thank them first. They all listened.

In many ways supervisors come into this category, but theirs is a more tangible contribution. They offer advice when needed, keep calm (and cheerful) in the face of apparent tragedy and have an endless supply of enthusiasm and fresh ideas. Eric Priest did a wonderful job in this role. My thanks to him are almost as boundless as my relief in getting it all over with.

This relief is probably also shared by my family, without whom none of this could have happened. They deserve much of my thanks: they have had to live with this thesis too. Having thesis-writing offspring must be a great trial for any mother, but my own coped admirably.

And finally my husband Andrew. Well, what can I say ? Blame him for any typos.

CERTIFICATE

I certify that Moira Mary Jardine has satisfied the conditions of the Ordinance and Regulations and is thus qualified to submit the accompanying application for the degree of Doctor of Philosophy.

Signature of Supervisor .....

Date 14.10.88

DECLARATION

I, Moira Mary Jardine, declare that the following thesis is a record of research work carried out by me, that the thesis is my own composition, and that it has not been submitted in any previous application for a higher degree.

Signature of Candidate .....

Date 14th December 1988

POSTGRADUATE CAREER

I was admitted into the University of St. Andrews as a research student under Ordinance General No. 12 in October 1985 and as a candidate for the degree of Ph. D. in October 1986, to work on aspects of magnetic reconnection under the supervision of Professor E.R. Priest.

COPYRIGHT

In submitting this thesis to the University of St. Andrews I understand that I am giving permission for it to be made available for use in accordance with the regulations of the University Library for the time being in force, subject to any copyright vested in the work not being affected thereby. I also understand that the title and abstract will be published, and that a copy of the work may be made and supplied to any *bona fide* library or research worker.

CHAPTER 1

INTRODUCTION

1.1 The process of magnetic reconnection

Studies of magnetic field reconnection have been pursued for many years now, but there still remains a great deal to be learned about this fundamental physical process. Its importance lies in its ability to release stored magnetic energy, changing the topology of the field and allowing lower energy states to be accessed. It is thought to be important in many different phenomena, both in astrophysics and the laboratory (for reviews see, for example: Hones, 1984; Priest, 1984, 1985). To mention a few examples, it may be occurring in solar flares, at the dayside magnetopause and in the geomagnetic tail (see, e.g. Forbes & Priest, 1982) . A little further from home, it may become important during star formation and in stellar coronae (Mestel, 1985; Bonnet and Dupree, 1981) and in more exotic topics such as structure in jets and magnetic viscosity in accretion discs (Asseo & Sol, 1986) .

Reconnection of magnetic field lines occurs in small regions of high magnetic field gradient, where the 'frozen in' approximation breaks down and the field diffuses through the plasma. Thus, when as shown in Figure 1.1, two regions of oppositely directed field lines are brought together, reconnection can occur in the current sheet (or diffusion region) which forms between them. The newly reconnected field lines are highly curved and accelerate plasma away from the diffusion region at approximately the Alfvén speed. Thus, although the reconnection takes place in a very small region, the resulting reconfiguration of the field lines affects the global structure of the magnetic field and releases energy from it into the thermal and kinetic energy of the plasma.

Emanating from the diffusion region are two pairs of slow-mode shocks; these cannot propagate in a direction perpendicular to the field and so stand in the flow, increasing the velocity and decreasing the magnetic field strength of the plasma which flows through them. In what follows we shall consider these shocks to divide the region of study into

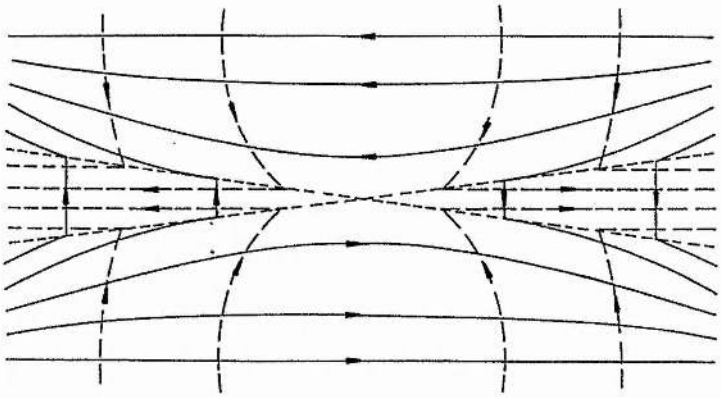

Figure 1.1: Fieldlines (solid) and streamlines (dashed) in Petschek's reconnection model.

two parts: an upstream part, where the field lines are moving towards the diffusion region and a downstream part where they are moving away from it.

The early models of reconnection have been reviewed several times (see e.g. Sonnerup, 1979; Hones, 1984; Priest, 1985; Shivamoggi, 1985) and we will not attempt to repeat this here. What we shall do instead is to summarise briefly those papers which are of particular relevance to the work in this thesis.

1.2 Some basic definitions

Before embarking on a mathematical description of the reconnection process, it is worth gathering together the basic equations and definitions that will be used in the rest of this thesis. All of the models that we will be discussing are based on the MHD equations. Thus, for a compressible, steady-state, infinitely conducting plasma, we have:

$$\nabla \cdot \boldsymbol{B} = 0 \tag{1.1}$$

$$\boldsymbol{E} = -\boldsymbol{v} \times \boldsymbol{B} \tag{1.2}$$

$$(\boldsymbol{v} \cdot \nabla)\rho + \rho(\nabla \cdot \boldsymbol{v}) = 0 \tag{1.3}$$

$$\rho(\boldsymbol{v} \cdot \nabla)p - \gamma p(\boldsymbol{v} \cdot \nabla)\rho = 0 \tag{1.4}$$

$$\rho(\boldsymbol{v} \cdot \nabla)\boldsymbol{v} = -\nabla p - \nabla\left[\frac{B^2}{2\mu}\right] + (\boldsymbol{B} \cdot \nabla)\frac{\boldsymbol{B}}{\mu} \tag{1.5}$$

Equations (1.1), (1.3) and (1.5) describe the conservation of flux, mass and momentum; (1.2) is a simplified Ohm's law (which becomes $\boldsymbol{E} + \boldsymbol{v} \times \boldsymbol{B} = \boldsymbol{j}/\sigma$ if finite resistivity is included) and (1.4) is an adiabatic energy equation. Written in another way, (1.4) becomes

$$(\boldsymbol{v}.\boldsymbol{\nabla})\frac{p}{\rho^\gamma} = 0$$

which states that p/ρ^γ is a constant on a streamline. Equation (1.4) can also be written in conservation form:

$$\boldsymbol{\nabla}.\left[(\frac{\gamma}{\gamma-1}p + \tfrac{1}{2}\rho v^2)\boldsymbol{v} + \frac{\boldsymbol{E}\times\boldsymbol{B}}{\mu}\right] = 0, \tag{1.6}$$

where $\gamma p/(\gamma-1) = p + e$ is the enthalpy, e is the internal energy per unit mass and $\boldsymbol{E}\times\boldsymbol{B}/\mu$ is the Poynting flux. Here, we have neglected ohmic heating and losses due to radiation and conduction. Finally, we can write the current explicitly as

$$\mu\boldsymbol{j} = \boldsymbol{\nabla}\times\boldsymbol{B}$$

In (1.4) and (1.6) $\gamma = c_p/c_v$ is the ratio of specific heats. We shall also use the following definitions:

1. the sound speed, c_s, is given by:

$$c_s = \left(\frac{\gamma p}{\rho}\right)^{1/2};$$

2. the plasma beta, which is the ratio of plasma to magnetic pressure, is given by:

$$\beta = \frac{2\mu p}{B^2};$$

3. the Alfvén speed is:

$$v_A = \frac{B}{(\mu\rho)^{1/2}};$$

4. the magnetic Mach number is:

$$M = \frac{v}{v_A}$$

(where v is a typical plasma speed);

5. the magnetic Reynolds number is:

$$R_{me} = \frac{Lv}{\eta}$$

(where η is the magnetic diffusivity)

6. the internal energy per unit mass is:

$$e = c_v T = \frac{p}{(\gamma - 1)\rho}; \text{ and} \tag{1.7}$$

7. the equation of state is:

$$p = \frac{k_B \rho T}{m}$$

(where k_B is Boltzmann's constant and m is the mean particle mass).

If the plasma is incompressible, there are no density variations and these basic equations take a different form. The incompressible limit can be obtained rigorously by taking $c_s/v \to \infty$ (or, equally, $\gamma \to \infty$). Thus, (1.1), (1.2) and (1.5) are unchanged, while, assuming that the pressure perturbations are finite, (1.4) gives

$$(\boldsymbol{v}.\nabla)\rho = 0. \tag{1.8}$$

Thus, (1.3) becomes

$$\nabla.\boldsymbol{v} = 0. \tag{1.9}$$

and we find that pressure perturbations are no longer associated with density perturbations. From the steady-state adiabatic heat equation:

$$\rho(\boldsymbol{v}.\nabla)e - \frac{p}{\rho}(\boldsymbol{v}.\nabla)\rho = 0 \tag{1.10}$$

we can see that, in the incompressible limit, if p and ρ are finite, then there will be no changes in the internal energy following the flow. In this case, the energy equation simply reduces to the equation of motion (1.5). In addition, since from (1.10) and (1.8) we know that

$$\nabla.(e\boldsymbol{v}) = 0 \tag{1.11}$$

then (1.6) becomes:

$$\nabla.\left[(p + \tfrac{1}{2}\rho v^2)\boldsymbol{v} + \frac{\boldsymbol{E} \times \boldsymbol{B}}{\mu}\right] = 0, \tag{1.12}$$

Although setting $\gamma \to \infty$ does recover the incompressible forms of the above equations, this is purely a mathematical device, since in reality γ is of order one. Another way of obtaining this limit is to note that if $\beta \gg 1$ then, since $c_s^2/v_A^2 = \gamma\beta/2$, this implies that $v_A \ll c_s$. If all the plasma speeds are very much less than the Alfvén speed, this in turn implies that $v \ll v_A \ll c_s$. Thus, if β is large, we would expect the plasma to behave as if it were incompressible. This does not, of course, mean that in an incompressible plasma β *has* to be large: it would equally well be possible to have $v \ll c_s$ and $v_A/c_s = O(1)$.

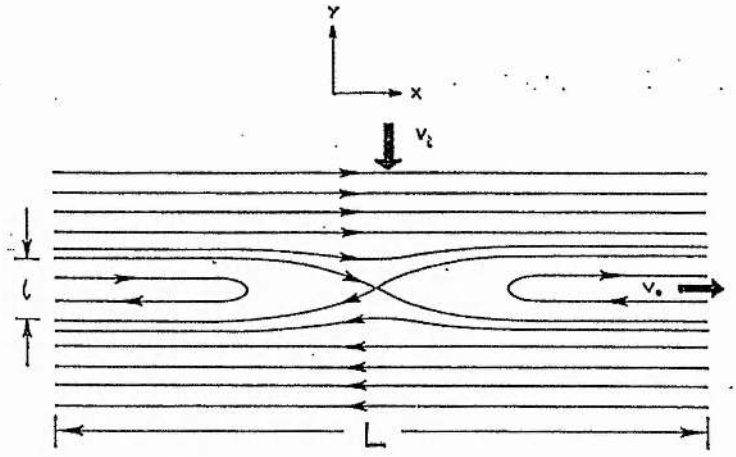

Figure 1.2: The Sweet-Parker model of reconnection.

If we use $\beta \to \infty$ to obtain the incompressible limit, then we will have an incompressible plasma *in which* β *is large.* This is rather different from taking the limit $\gamma \to \infty$, where we could have an incompressible plasma with β arbitrary.

1.3 Previous models

Studies of magnetic reconnection can be traced back to the early the models of Sweet (1958) and Parker (1963) . Here, the magnetic field is annihilated in a current sheet formed when two regions of oppositely directed magnetic fields are brought together. If p_i and p_0 are the pressures at the inflow and outflow of the sheet ($x = 0$, $|y| = \ell/2$ and $|x| = L/2$, $y = 0$ in Figure 1.2) and p_N is the pressure at the neutral point ($x = 0$, $y = 0$), then pressure balance across the sheet requires that

$$p_i + \frac{B_i^2}{2\mu} = p_N$$

For the outflowing plasma, Bernoulli's equation gives (since, to lowest order, there is no magnetic field)

$$p_N = p_0 + \frac{\rho v_0^2}{2}$$

Equating the inflow and outflow pressures gives the outflow speed as

$$v_0 = \frac{B_i}{(\mu\rho)^{1/2}} = v_{Ai}$$

Thus plasma flows out of the current sheet at a speed equal to the Alfvén speed at the inflow.

Assuming incompressibility, conservation of mass gives

$$\frac{\ell}{L} = M_i \tag{1.13}$$

such that, for small reconnection rates, the current sheet is long and thin. The width of the sheet is determined by a balance between the rate at which the magnetic field is convected in and the rate at which it diffuses away. It is given by

$$\ell = \frac{\eta}{v_i}$$

Thus from (1.13)

$$M_i = R_{mi}^{-1/2} \tag{1.14}$$

where $R_{mi} = Lv_{Ai}/\eta$.

This highlights the main problem with the Sweet-Parker model. For most astrophysical applications, the global scale length, L_e (which in this model is equal to the length of the current sheet, L) is very large and correspondingly the reconnection rate M_i is very small.

This difficulty was overcome by Petschek (1964) who realised that slow-mode shocks (or their incompressible equivalent, discrete slow-mode compressions) would emanate from the diffusion region (see Figure 1.1). These stand in the flow, decreasing the magnetic field strength and increasing the velocity of the plasma which flows through them. The boundary layer between these two shocks is very thin and so, from 1.1

$$B_x \gg B_y$$

and

$$\frac{\partial B_x}{\partial y} \gg \frac{\partial B_y}{\partial x}$$

Petschek assumed that

1. the outflow velocity is a function only of x;

2. pressure gradients can be neglected;

3. the plasma is incompressible

and obtained from the y-component of (1.5)

$$\rho v_i v_0 = \frac{B_i B_0}{\mu}$$

Thus, since from the steady-state assumption, the electric field is uniform, we have $v_i B_i = v_0 B_0$ and so the outflow velocity is just v_{Ai}. This is just equal to that from the Sweet-Parker current sheet, although in that case, the plasma acceleration was due to the action of pressure forces, whereas in this case it is due to the tension in the reconnected field lines.

Petschek then calculated the field *outside* the boundary layer by noting that since the magnetic field inside is known (and the normal component of the field must be conserved across the shock), then the normal component of the field on the inflow boundary of the shock is also known. Since the magnetic field in the inflow is potential this is sufficient to specify the inflow field.

In Petschek's model, then, the diffusion region could be much smaller than the global scale length and so much larger reconnection rates could be achieved. Petschek estimated the maximum reconnection rate possible with this model by evaluating the change in the magnetic field strength as it approached the diffusion region. He found that

$$B_i = B_e - \frac{4}{\pi} M_e B_e \ln\left(\frac{L_e}{L}\right)$$

Putting $B_i = B_e/2$ gave Petschek a maximum reconnection rate of

$$M_e^* = \frac{\pi}{8 \ln R_{me}}$$

which is much larger than the Sweet-Parker value and lies between 0.01 and 0.1.

One extension of Petschek's model which is particulary relevant to the work in the next few chapters is that by Green & Sweet (1967) . They considered the effects of a non-uniform inflow and concluded that if the inflow magnetic field *decreases* with distance from the y-axis, then the downstream field will be curved in a direction opposite to that in Figure 1.1. This requires a reversal of the tangential magnetic field direction at the shock, but, as shown by Kantrowitz and Petschek (1966) there are no stable, physical solutions of the conservation equations for shock waves with this property. Green and Sweet concluded from this, that, in the generalised case of a non-uniform inflow, Petschek's solution is invalid.

Petschek and Thorne (1967) resolved this difficulty by suggesting that in cases where the downstrean solution required a reversal in B_t that this could be achieved by finite-amplitude intermediate waves which would stand in the flow, ahead of the slow shocks. These waves would also be required if there was a component of the field out of the $x-y$ plane, or if there was an asymmetry across the x-axis.

More recently, the effects of asymmetries have been investigated by Semenov *et al.* (1983b) and Heyn *et al.* (1986,1988:preprint). They find that rotational (Alfvén) waves, slow shocks, rarefaction waves (expansion fans) and a contact discontinuity may occur, depending on the inflow conditions. Also, Semenov *et al.* (1983a) have produced a compressible form of Petschek's model, including a lowest-order downstream solution.

Even higher reconnection rates than those in Petschek's model (possibly of order one) were proposed by Sonnerup (1970) (see also the family of models by Yeh and Axford (1970) of which Sonnerup's is the only nonsingular member). In this case, the inflowing field lines are straight, rather than curved as in Petschek's model, and the necessary change in their direction is accomplished by *two* sets of waves: discrete slow-mode compressions similar to Petschek's and, upstream of these, slow-mode expansion waves. Although this model has the advantage that it is exact, it has the disadvantage that the expansion waves must be generated at corners in the inflow region. They travel inwards to intersect at the diffusion region. It is difficult to think of a physical situation in which this would arise naturally.

Vasyliunas (1975) suggested that a Sonnerup-like solution could be achieved with a slow-mode expansion spread throughout the inflow region. In Petschek's model, on the other hand, the inflow undergoes a fast-mode expansion and Vasyliunas suggested that the differences between the two models could be understood in terms of differences in their inflow regions. If, as in these cases, the density is uniform, then the ratio of the magnetic field strength to the length of a field line is a constant (since $\overline{B}/l = \overline{\rho}$). For Petschek-like reconnection (see Figure 1.1) he assumed that as the plasma flows in towards the diffusion region, the field strength is uniform at either side of the region, but decreases on the axis. Thus l decreases and the streamlines must converge. The pressure is, however, also uniform at either side, so it must decrease on the axis. The fact that this fall in pressure is linked with a decrease in magnetic field strength means that this is a *fast-mode expansion.* On the other hand, for Sonnerup-like reconnection, the field is uniform on the axis, but increases at either side. Thus l increases and the streamlines must diverge. Since the pressure is also uniform on the axis, this means that there must be a pressure drop on either side. Hence, since we have a fall in pressure linked with an increasing magnetic field, this is a *slow-mode expansion.*

This idea, that different reconnection regimes result from different inflow conditions was explored further by Priest & Forbes (1986) who developed a whole family of incompressible models of which Petschek-like and Sonnerup-like soutions are particular cases.

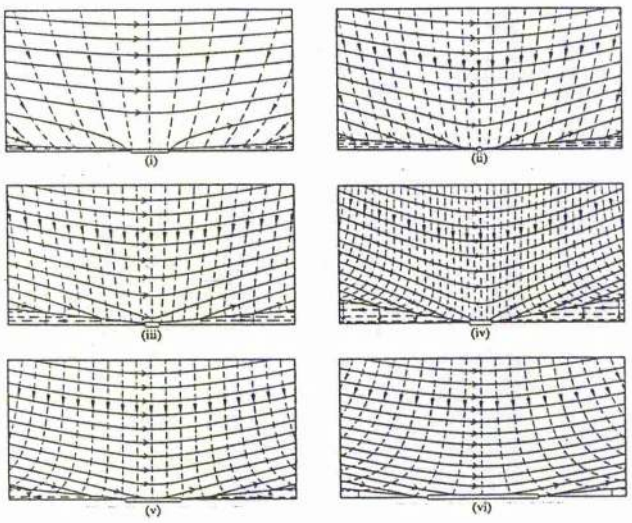

Figure 1.3: Different classes of solution (from Priest & Forbes 1986).

The different members of the family are characterised by a parameter b_0, which essentially is a measure of the transverse velocity on the inflow boundary. For example, $b_0 = 0$ gives a Petschek-like solution, $b_0 = 1$ gives a Sonnerup-like solution and $0 < b_0 < 1$ gives a hybrid regime with a fast-mode expansion on the y-axis and a slow-mode expansion at the edges ($|x| = 1$) of the system (see Figure 1.3). Also, $b_0 < 0$ gives slow-mode compressions with slower reconnection rates , while $b_0 > 1$ produces slow-mode expansions known as a 'flux pile-up' regime, in which the reconnection rate can be faster, the diffusion region is long and the flow diverges as it comes in.

In the limit as b_0 becomes very much greater than one (although here nonlinear effects become important) it seems that the solutions tend towards the stagnation point flow solution of Sonnerup and Priest (1975) (see also Parker (1963) and Priest and Sonnerup (1975)). This is an exact solution of the resistive MHD equations for field annihilation in a current sheet. The field lines are straight and the flow diverges as it comes in, forming a stagnation point at the neutral point. The reconnection rate is arbitrarily large and there is both a slow-mode expansion at low values of y and a fast-mode compression, associated with nonlinear effects, at large values of y.

More recently, Gratton *et al.* (1988) have generalised the stagnation point flow solutions to allow for viscous effects, while Heyn *et al.* (1988, preprint) have introduced a normal component of the magnetic field as a perturbation and solved the resulting equations

numerically.

The Priest-Forbes family of models has therefore been an important step in our understanding of previous reconnection models and their relation to each other. Since it forms the basis for much of the work in this thesis, we will devote the next section to a brief summary of the method and results.

1.4 The Priest-Forbes family of reconnection models

We here review briefly the main features of the Priest & Forbes model of reconnection, whose inflow region occupies the region $|x| \leq 1$, $0 \leq y \leq 1$. The solution is obtained by expanding the basic MHD equations for an incompressible plasma (see (1.1), (1.2), (1.5) and (1.9)) in powers of the inflow Mach number, M_e, such that

$$\boldsymbol{v} = \boldsymbol{v}_0 + \epsilon \boldsymbol{v}_1 + \epsilon^2 \boldsymbol{v}_2 + \cdots,$$

where $v_1/v_0 = O(1)$ etc. and ϵ is a small parameter of order M_e. Expanding about a uniform magnetic field ($\boldsymbol{B}_0 = B_{0x}\hat{\boldsymbol{x}}$) and a stationary plasma ($v_0 = 0$) in the inflow region therefore gives as a solution of (1.1) to (1.4) for the magnetic field, electric current, plasma pressure and plasma velocity:

$$\overline{B}_{1x} = \sum_{n=0}^{\infty} a_n \sinh\left[(n+\tfrac{1}{2})\pi(1-y)\right]\left\{b_n - \cos\left[(n+\tfrac{1}{2})\pi x\right]\right\}, \tag{1.15}$$

$$\overline{B}_{1y} = \sum_{n=0}^{\infty} a_n \cosh\left[(n+\tfrac{1}{2})\pi(1-y)\right]\sin\left[(n+\tfrac{1}{2})\pi x\right], \tag{1.16}$$

$$\mu\vec{j}_1 = \sum_{n=0}^{\infty} a_n b_n (n+\tfrac{1}{2})\pi \cosh\left[(n+\tfrac{1}{2})\pi(1-y)\right], \tag{1.17}$$

$$\overline{p}_1 = -\frac{2}{\beta_e}\sum_{n=0}^{\infty} a_n b_n \sinh\left[(n+\tfrac{1}{2})\pi(1-y)\right], \tag{1.18}$$

$$\overline{v}_{2y} = M_e B_{1x}, \tag{1.19}$$

$$\overline{v}_{2x} = -M_e\left[\overline{B}_{1y} - \mu\vec{j}_1 x\right], \tag{1.20}$$

where

$$a_n = \frac{4M_e \sin\left[(n+\tfrac{1}{2})\pi L\right]}{L(n+\tfrac{1}{2})^2\pi^2 \cosh\left[(n+\tfrac{1}{2})\pi\right]}, \tag{1.21}$$

We have re-cast these equations in the dimensionless variables $\overline{B} = B/B_e$, $\overline{v} = v/v_{Ae}$, $\overline{p} = p/p_e$, $\overline{j} = j/B_e$ and $\overline{\rho} = \rho/\rho_e$. We identify B_0, v_1, p_0 and ρ_0 with the values of the magnetic field strength, velocity and pressure at large distances from the diffusion region and denote them by a subscript e (e.g. $B_0 = B_e$).

B_N is given by $M_e B_e$, L is the length of the diffusion region and the global scale length (L_e) is taken as unity. As noted by Jardine & Priest (1988a) the second-order magnetic field component may then be obtained from the solution of

$$\nabla^2 B_{2y} = -\frac{\mu B_{1y}}{B_{0x}^2}\frac{d^2 p_1}{dy^2}$$

As can be seen from (1.15), (1.17), (1.18), or (1.20), the boundary conditions on the sides $x = \pm L_e$, namely the functional forms of B_{1x}, j_1, p_1 or v_{2x}, determine the values of the constants b_n. In particular, we here follow Priest & Forbes in setting $b_n = b_0$ for all n. An important point to note about these solutions is that, because of the method used (a perturbation about straight field lines), they are only valid for field lines with a small degree of curvature, of the order of M_e. Because the discrete slow-mode compression can only advance into the plasma at a speed proportional to the normal component of the magnetic field, B_N, the position at which the wave will be stationary depends on the curvature of the upstream magnetic field. As a result, we would expect the wave to advance a distance of the order of M_e, which will therefore define the width of the downstream region.

One further remark about these solutions concerns the boundary conditions used i.e.

1. B_{1x} even in x (and therefore B_{1y} odd in x)
2. $\partial B_{1y}/\partial x = 0$ on $x = 1$
3. $B_{1x} = 0$ on $y = 1$
4. $B_{1y} = f(x)$ on $y = 0$

where

$$\begin{aligned} f(x) &= 2B_N && L \le x \le 1 \\ &= 2B_N x/L && 0 \le x \le L \end{aligned}$$

This choice of B_N was made from considerations of the speed of the shocks. It is used to determine the value of a_n and will be used later in the jump relations.

Using these solutions, Priest and Forbes were able to evaluate the field strength at the entrance to the diffusion region, B_i, from

$$\begin{aligned} B_i &= B_e + B_{1x}(0,0) \\ &= B_e + \sum_{n=0}^{\infty} a_n (b_0 - 1)\sinh[(n+\tfrac{1}{2})\pi]. \end{aligned} \tag{1.22}$$

Now, since the electric field is uniform,

$$v_i B_i = v_e B_e \tag{1.23}$$

and

$$M_i = M_e \left(\frac{B_e}{B_i}\right)^2 \tag{1.24}$$

Hence, for each value of b_0 there is a unique relationship between M_e and M_i. Thus, for solutions with $b_0 < 1$ there is a maximum value of M_e, while for solutions with $b_0 > 1$ there is a maximum value of M_i. For the case $b_0 = 1$ there is no change in the magnetic field on the y-axis and so $B_i = B_e$.

The length of the diffusion region can also be calculated from (1.24). The balance of diffusion and convection of magnetic field lines within the diffusion region gives its thickness as

$$\ell = \eta / v_i \tag{1.25}$$

while mass conservation gives

$$L v_i = \ell v_{Ai} \tag{1.26}$$

Eliminating ℓ from (1.25) and (1.26) gives for the length of the diffusion region:

$$L = \frac{\eta v_{Ai}}{v_i^2}$$

or, from (1.23)

$$L = \frac{\eta v_{Ae} B_i^3}{v_e^2 B_e^3}$$

Thus (1.24) gives

$$L = \frac{1}{R_{me} M_e^{1/2} M_i^{3/2}} \tag{1.27}$$

The main result, then, from this piece of work is that the inflow boundary conditions are crucial in determining the type of reconnection which is taking place and hence not only the form of the solutions but also the reconnection rate itself.

CHAPTER 2

WEAKLY NONLINEAR THEORY

2.1 Introduction

The demonstration by Priest and Forbes of the role of the external boundary conditions in determining the reconnection regime raises some important questions about the reconnection process. For example, given that the upstream boundary conditions determine the form of the upstream solution and the reconnection rate, what is the role of the downstream boundary conditions? In some numerical experiments (e.g. Biskamp (1986)) conditions are specified at both the upstream and the downstream boundaries and certainly the results do not appear to resemble those of analytical models. Another question then might be whether we are free to prescribe anything downstream and if so, what are the effects of different choices? How does the choice of inflow parameters affect the downstream solution?

In this chapter we shall answer these questions by finding a solution for the downstream region and matching it to the existing upstream solution. This matching is carried out using the jump relations across the wave which separates the two regions. These coupled solutions then give a global picture of the reconnection process and show not only how the downstream region responds to changes in the inflow, but also how altering the downstream boundary conditions affects the result.

2.2 The downstream region

For this region also we expand (1.1), (1.2), (1.5) and (1.9) in powers of M_e, in this case about a uniform flow with $v_{0x} = v_{Ae}$, the external Alfvén speed. In addition, since the width of the region will be of order M_e, we rescale the y-coordinate as $y = \epsilon y'$, where ϵ is a small parameter of order M_e. The resulting formidable set of equations can be reduced to a tractable form as follows. From equations (1.1) and (1.9) we deduce that B_{0y} is only

a function of x (as indeed are v_{0y} and v_{1y}, although in this case symmetry demands that these are both zero everywhere). Then, using the result from the jump relations that $B_{0y} = 0$ on $y = M_e x$ (i.e. at the wave), (1.2) implies that

$$B_{0y} = 0 \tag{2.1}$$

and

$$B_{1y} = M_e B_e \tag{2.2}$$

(and hence from (1.1) $B_{0x} = B_{0x}(y)$).

The y-component of (1.5) gives $p_0 + B_{0x}^2/2\mu = c_1$, a constant (again using the jump relations) and hence $p_0 = p_0(y)$. The x-component gives $dB_{0x}/dy = 0$ and hence from symmetry

$$B_{0x} = 0 \tag{2.3}$$

and

$$p_0 = c_1, \tag{2.4}$$

while finally

$$p_1 = p_1(x), \tag{2.5}$$

which is therefore determined by the jump relations.

We may therefore reduce the expanded forms of (1.5) to (1.1) to five equations:

$$\frac{\partial v_{1x}}{\partial x} = -\frac{1}{\rho v_{Ae}}\frac{dp_1}{dx} + \frac{M_e}{(\mu\rho)^{1/2}}\frac{\partial B_{1x}}{\partial y}, \tag{2.6}$$

$$v_{1x} = -\frac{1}{M_e(\mu\rho)^{1/2}}B_{2y}, \tag{2.7}$$

$$\frac{\partial v_{1x}}{\partial x} = -\frac{\partial v_{2y}}{\partial y}, \tag{2.8}$$

$$\frac{\partial B_{1x}}{\partial x} = -\frac{\partial B_{2y}}{\partial y}, \tag{2.9}$$

$$\frac{\partial}{\partial y}\left[p_2 + \frac{B_{1x}^2}{2\mu}\right] = 0. \tag{2.10}$$

From (2.7), (2.9) and (2.6) we can obtain a single equation for B_{1x},

$$\frac{\partial^2 B_{1x}}{\partial x^2} - M_e^2\frac{\partial^2 B_{1x}}{\partial y^2} = 0, \tag{2.11}$$

which has the general solution

$$B_{1x}(x,y) = f(y - M_e x) + g(y + M_e x), \tag{2.12}$$

where f and g are arbitrary functions.

The particular form of this solution, in which the jump relations are used as a boundary condition on the wave, is outlined in Appendix A. The essential result, in the limit ($L \ll 1$) where the length of the diffusion region and hence its influence on the downstream solution is negligible, is that over the greater part of the downstream region:

$$\begin{aligned} B_{1x}(x,y) &= B^u_{1x}\left[\frac{1}{2M_e}(y+M_e x)\right] - B^u_{1x}\left[\frac{1}{2M_e}(y-M_e x)\right] \\ &= \sum_{n=0}^{\infty} a_n \sinh\left[(n+\tfrac{1}{2})\pi\right]\left\{-\cos\left[\frac{(n+\frac{1}{2})\pi(y+M_e x)}{2M_e}\right]\right. \\ &\quad \left.+\cos\left[\frac{(n+\frac{1}{2})\pi(y-M_e x)}{2M_e}\right]\right\} \end{aligned} \tag{2.13}$$

and

$$\begin{aligned} v_{1x} &= \frac{1}{(\mu\rho)^{1/2}}\left\{B^u_{1x}\left[\frac{1}{2M_e}(y+M_e x)\right]\right. \\ &\quad \left.+B^u_{1x}\left[\frac{1}{2M_e}(y-M_e x)\right] - B^u_{1x}(x)\right\} \\ &= \frac{1}{(\mu\rho)^{1/2}}\sum_{n=o}^{\infty} a_n \sinh\left[(n+\tfrac{1}{2})\pi\right]\left\{b_0 - \cos\left[\frac{(n+\frac{1}{2})\pi(y+M_e x)}{2M_e}\right]\right. \\ &\quad \left.-\cos\left[\frac{(n+\frac{1}{2})\pi(y-M_e x)}{2M_e}\right] + \cos\left[(n+\tfrac{1}{2})\pi x\right]\right\}, \end{aligned} \tag{2.14}$$

where a superscript u refers to a quantity measured just upstream of the wave, on $y = 0$ of the upstream solution. In addition, we have from the jump relations:

$$p_0 = p_e + \frac{B_e^2}{2\mu}, \tag{2.15}$$

and (2.16)

$$\begin{aligned} p_1 &= p_1^u + \frac{B_e}{\mu}B^u_{1x} \\ &= -\frac{B_e}{\mu}\sum_{n=0}^{\infty} a_n \sinh\left[(n+\tfrac{1}{2})\pi\right]\cos\left[(n+\tfrac{1}{2})\pi x\right], \end{aligned} \tag{2.17}$$

while Ampère's law ($j = \nabla \times B/\mu$) gives

$$\mu j_0 = -\frac{\partial B_{1x}}{\partial y}$$

and hence from (2.13)

$$\begin{aligned} \mu j_0 &= -\frac{1}{2M_e}\sum_{n=o}^{\infty} a_n(n+\tfrac{1}{2})\pi \sinh\left[(n+\tfrac{1}{2})\pi\right]\left\{\sin\left[\frac{(n+\frac{1}{2})\pi(y+M_e x)}{2M_e}\right]\right. \\ &\quad \left.-\sin\left[\frac{(n+\frac{1}{2})\pi(y-M_e x)}{2M_e}\right]\right\}. \end{aligned} \tag{2.18}$$

We may also find v_{2y} from (2.6) and (2.8):

$$v_{2y}(x,y) = \frac{y}{\rho v_{Ae}} \frac{dp_1}{dx} - \frac{M_e}{(\mu\rho)^{1/2}} B_{1x}, \tag{2.19}$$

while (2.7) gives

$$B_{2y}(x,y) = M_e(\mu\rho)^{1/2} v_{1x}, \tag{2.20}$$

where arbitrary functions of integration have been removed by invoking symmetry or by using the jump relations.

All that is needed now to complete the solution is a knowledge of the exact form of the jump relations and their role in linking the upstream and downstream solutions.

2.3 The jump relations

If we assume a steady-state, two-dimensional, incompressible plasma, then the jump relations may be obtained by integrating (1.1), (1.2),(1.5) and (1.9) across a one-dimensional wave to give (e.g. Jeffrey & Taniuti, (1964))

$$\left.\begin{aligned} v_n &= -v_{An}, \\ [v_n] &= 0, \\ [v_t] &= -\tfrac{1}{(\mu\rho)^{1/2}}[B_t], \\ [B_n] &= 0, \\ \left[p + \tfrac{B^2}{2\mu}\right] &= 0, \end{aligned}\right\} \tag{2.21}$$

where v_{An} is the Alfvén speed based on the normal component of the magnetic field, subscripts n and t refer to components normal to and transverse to the wave respectively and $[X]$ denotes the change in a quantity X on crossing the wavefront.

Writing these in terms of x and y-components and expanding in powers of M_e gives (see Appendix B for details)

$$\tan\alpha_0 = 0, \tag{2.22}$$

$$\tan\alpha_1 = M_e, \tag{2.23}$$

$$\tan\alpha_2 = \frac{B^u_{2y}}{B_e}, \tag{2.24}$$

$$v^d_{0y} = 0, \tag{2.25}$$

$$v^d_{1y} = 0, \tag{2.26}$$

$$\pm v^d_{2y} = -\frac{B^u_{2y}}{(\mu\rho)^{1/2}} - v^d_{1x} M_e - \frac{M_e B^u_{1x}}{(\mu\rho)^{1/2}}. \tag{2.27}$$

$$B^d_{0x} = 0, \tag{2.28}$$

$$\pm B^d_{1x} = B^u_{1x} - (\mu\rho)^{1/2} v^d_{1x}, \tag{2.29}$$

$$\pm B^d_{2x} = B^u_{2x} + (\mu\rho)^{1/2}(v^u_{2x} - v^d_{2x}), \tag{2.30}$$

$$B^d_{0y} = 0, \tag{2.31}$$

$$B^d_{1y} = M_e B_e, \tag{2.32}$$

$$B^d_{2y} = M_e(\pm B^d_{1x} - B^u_{1x}), \tag{2.33}$$

$$p^d_0 = p_e + \frac{B_e^2}{2\mu}, \tag{2.34}$$

$$p^d_1 = p^u_1 + \frac{B_e}{\mu} B^u_{1x}, \tag{2.35}$$

$$p^d_2 = p^u_2 + \frac{1}{2\mu}\left[2B_e B^u_{2x} + (B^u_{1x})^2 - (B^d_{1x})^2 + 3M_e^2 B_e^2\right], \tag{2.36}$$

where superscripts u and d refer to upstream and downstream, respectively, α is the angle made by the wave to the x-axis (see Figure 2.1(a)) and the $\pm$ signs refer to the orientation of $\boldsymbol{v}^d$ and $\boldsymbol{B}^d$ (see Figure 2.1(b)). Note the two possible downstream orientations, depending on whether $B_x > 0$ and $v_y < 0$ or $B_x < 0$ and $v_y > 0$. In order to decide which are the appropriate signs for the downstream solution obtained in Section 2.2(b), we note from equation (A.9) in Appendix A that

$$v^d_{1x} - \frac{B^d_{1x}}{(\mu\rho)^{1/2}} + \frac{p^d_1}{\rho v_{Ae}} = c_3,$$

a constant. A choice of the negative sign for B^d_{1x} in (2.29) would then give B^u_{1x} = a constant, which from (1.15) is clearly incorrect; choosing the positive sign gives instead v^d_{1x} = a constant. In addition, from (2.19) we have, using (2.29) and (2.35)

$$\begin{aligned} v^d_{2y} = {} & \frac{y}{(\mu\rho)^{1/2}} \frac{dB^u_{1x}}{dx} - \frac{M_e}{(\mu\rho)^{1/2}} \left\{ B^u_{1x}\left[\frac{1}{2M_e}(y + M_e x)\right] \right. \\ & \left. - B^u_{1x}\left[\frac{1}{2M_e}(y - M_e x)\right]\right\}, \end{aligned} \tag{2.37}$$

which is positive. Hence the downstream solution is of the form shown in Figure 2.2.

From (2.37) and (2.27) we may also find B^u_{2y}:

$$B^u_{2y} = M_e x \frac{dB^u_{1x}}{dx} - 2M_e B^u_{1x}. \tag{2.38}$$

From(2.24) this defines $\tan\alpha_2$ and hence, by integration (since $\tan\alpha = dy/dx$ on the wave) the value of α at every point on the wave and hence the wave shape. Thus the position of the wave is given by

$$\begin{aligned} y_1 &= M_e x \\ y_2 &= \frac{M_e}{B_e}\left(B^u_{1x} - 3\int B^u_{1x}\, dx\right) \end{aligned} \tag{2.39}$$

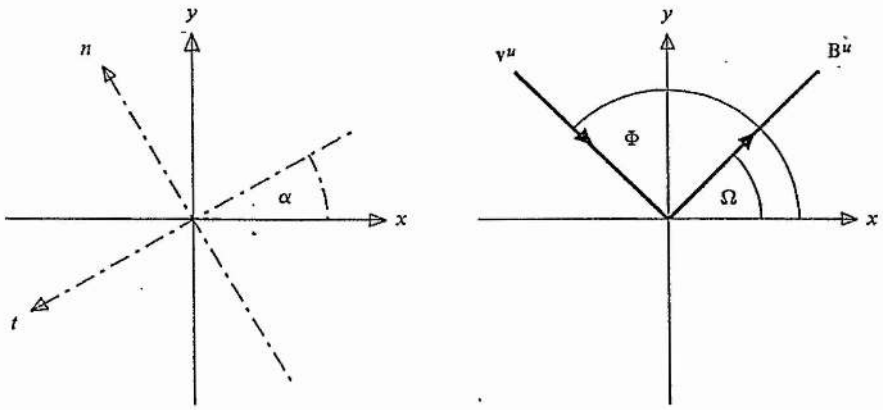

(a) *Upstream*

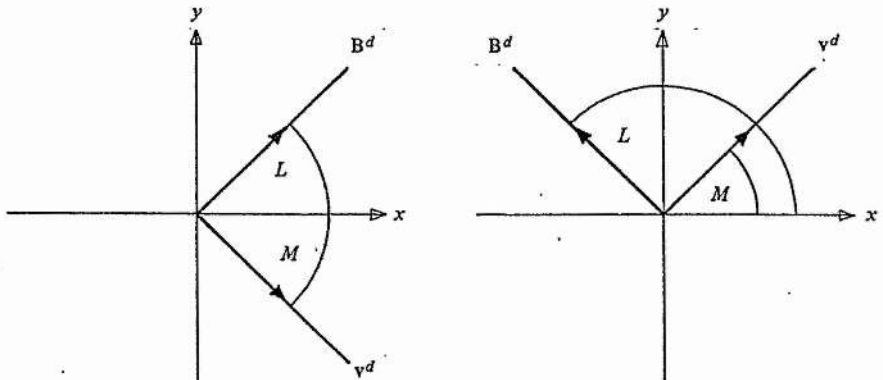

(b) *Downstream*

Figure 2.1: The magnetic field and plasma velocity vectors.
(a) Upstream, (b) downstream of the wave (where α is the angle made by the wave to the x-axis).

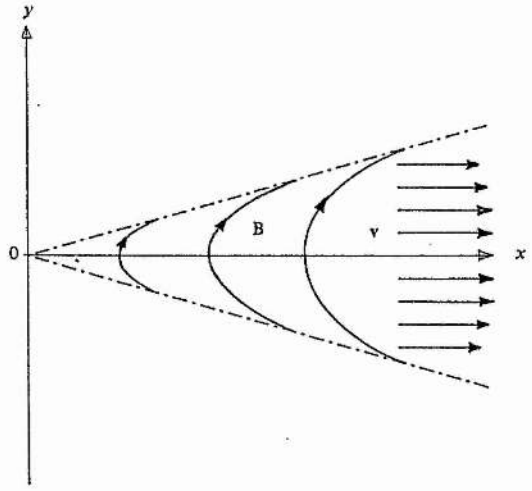

(a) Sketch of the field lines and flow velocity vectors in the downstream region.

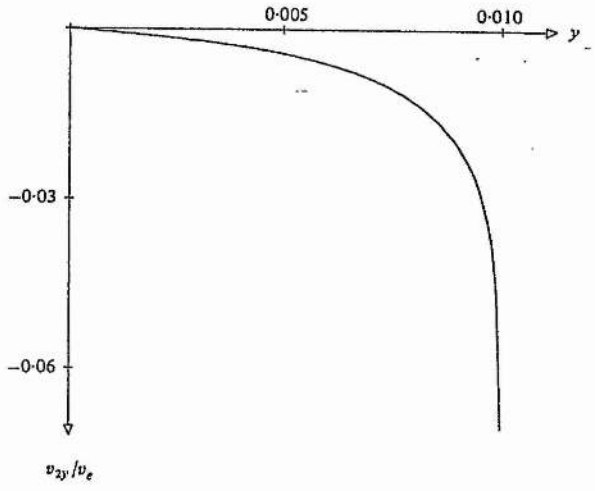

(b) Variation of the second-order y-component of velocity v_{2y} with y at $x = 1$.

Figure 2.2: The magnetic field and plasma velocity downstream.

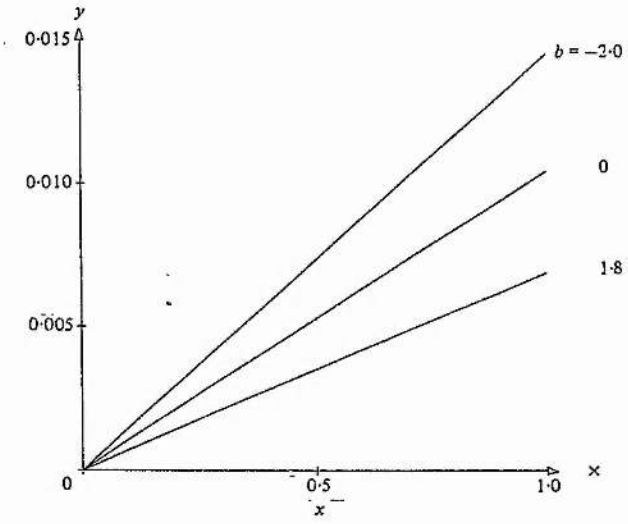

Figure 2.3: Variation of the shape of the discrete slow-mode compression with b_0.

$$= \frac{M_e}{B_e}\sum_{n=0}^{\infty} a_n \sinh\left[(n+\tfrac{1}{2})\pi\right]\left\{-2b_0 + \frac{3\sin[(n+\tfrac{1}{2})\pi x]}{(n+\tfrac{1}{2})\pi} - \cos[(n+\tfrac{1}{2})\pi x]\right\} \quad (2.40)$$

Figure 2.3 shows the resulting shape of the wave for several values of b_0.

2.4 The effect of varying upstream conditions

Now that we have the complete downstream solution to first order, it is possible to examine the response of the solution to changes in the upstream configuration. The general form of the downstream region is as shown in Figure 2.2(a). To first order, the streamlines are straight and the maximum velocity is attained on the x-axis (see Figure 2.4). We also find that the field lines are curved in such a way that the tension acts to propel plasma away from the diffusion region. This is in fact what would be expected from the work by Green & Sweet (1967) (see also comments in Chapter 1) since the upstream magnetic field strength always *increases* with x. To second order, the flow is converging (see Figure 2.2(b)). The lowest order current density is always negative, decreasing in magnitude with x from a maximum near the diffusion region and increasing close to the wave (see Figure 2.5). The perturbed pressure (p_1) also decreases with x, in this case to zero at x=1 (see Figure 2.6).

Surprisingly, perhaps, to first order, not only the pressure, but also the magnetic field and current density are independent of the type of upstream configuration. This can be

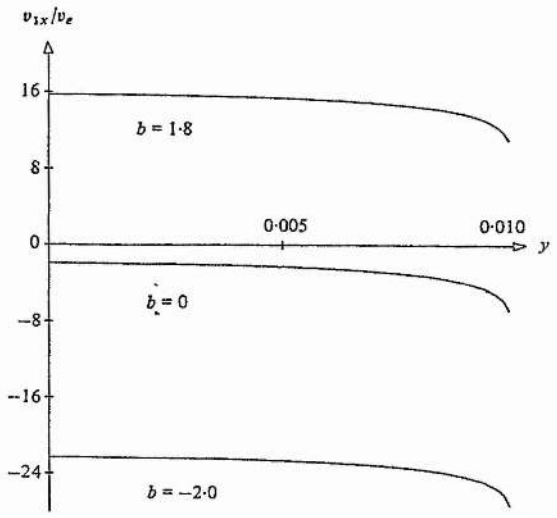

Figure 2.4: Profile of v_{1x} across the downstream region for several values of b_0.

seen quite clearly from equations (2.17), (2.13) and (2.18), which have no b_0-dependence. In addition, since v_{2y} involves only terms independent of b_0 (from (2.19)), it also will be insensitive to the form of the upstream solution. In fact, to first order, the only downstream variable which depends on b_0 is the velocity (v_{1x}): this increases in magnitude linearly with b_0 (see Figure 2.7) while retaining the same profile across the region shown in Figure 2.4. For $b_0 \geq 0.3$, we note that v_{1x} is positive and the downstream flow is greater than v_{Ae}, the Alfvén speed based on the upstream external magnetic field.

One other result of a variation of the upstream boundary conditions is a change in the curvature and the position of the wave. While to first order the wave is simply straight, to second order it appears curved and varies with b_0 as shown in Figure 2.3. As b_0 is increased through a slow compression to a flux pile-up regime, the wave closes down, making the downstream region narrower, and its curvature increases.

All this, of course, has immediate implications for the energy conversion process taking place as plasma flows through the reconnection site and its dependence on the particular upstream configuration. This will be discussed in Chapter 4

2.5 The effect of varying downstream conditions

While the downstream solution is certainly affected by the choice of upstream conditions, it is also sensitive to the choice of conditions downstream. From Section 2.3 it can be

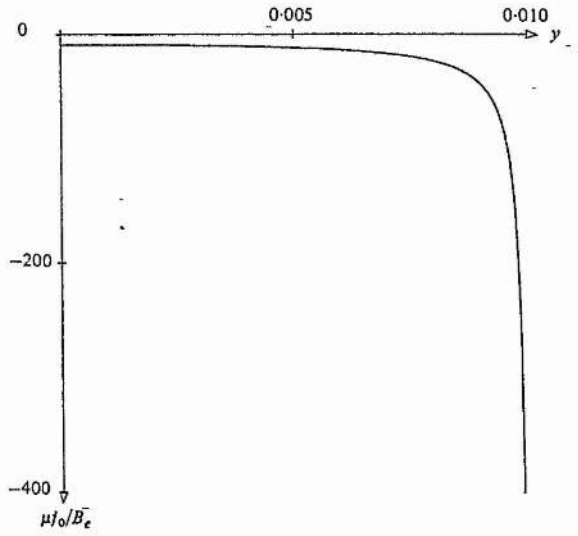

(a) Across the downstream region (with $x = 1$).

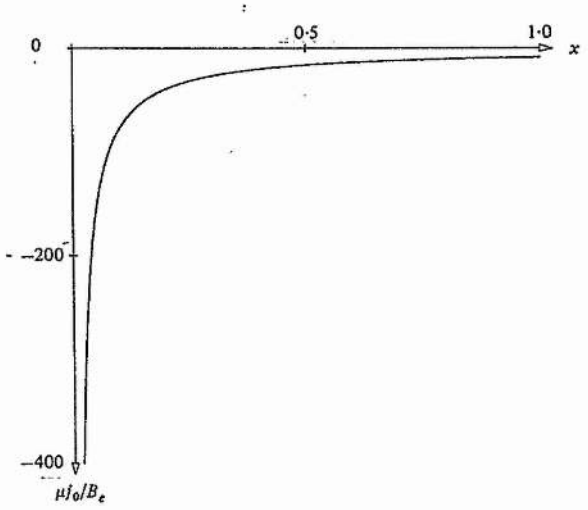

(b) Along the downstream region (with $y = 0$).

Figure 2.5: Variation of the electric current (μj_0) downstream.

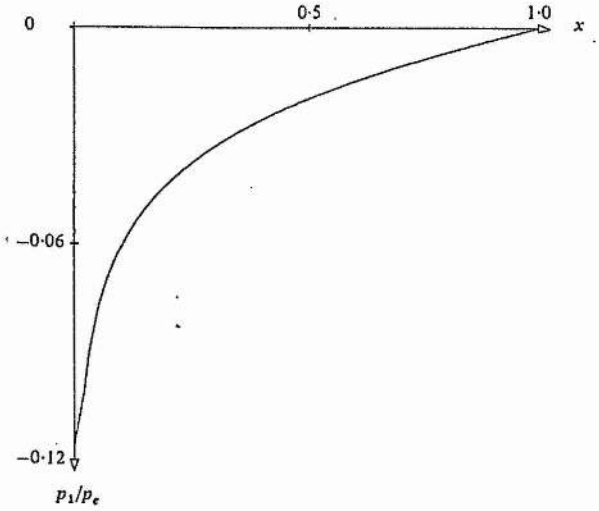

Figure 2.6: Variation of the perturbed pressure p_1 along the downstream region (with $y = 0$).

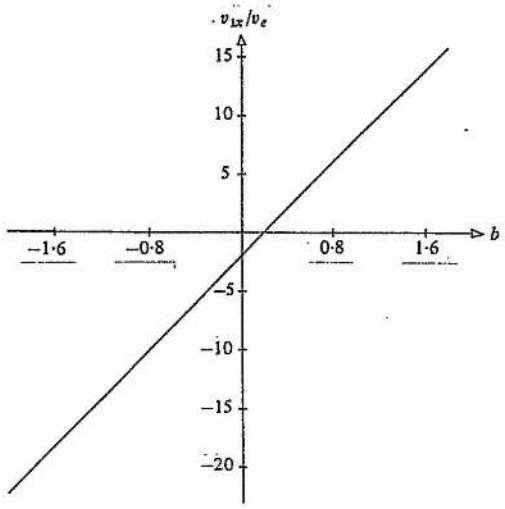

Figure 2.7: Variation with b_0 of the perturbed downstream velocity v_{1x}. The velocity is measured at $x = 1$, $y = 0$, and v_e is the upstream Alfvén speed.

seen that the five jump relations (2.21) will not determine the six unknowns downstream (the two components of velocity and magnetic field, pressure and wave position (α)) since v_x is arbitrary. To lowest order, we have taken this to be the external Alfvén speed, v_{Ae}, while the first-order choice is only restricted in our analysis to solutions which give a short diffusion region ($L \ll 1$), since in this case, $B_{1x} \simeq 0$ at $x = L$ and hence from (2.29) $v_{1x}^d \simeq B_{1x}^u(L,0)/(\mu\rho)^{1/2}$, which for $L \ll 1$ is just v_{Ai}, the Alfvén speed based on the magnetic field strength at the inflow to the diffusion region (for details see Appendix A). Hence the downstream solutions we have considered so far are in fact only a particular class for which these choices of v_{0x} and v_{1x} apply; a different choice would have given a different configuration.

In summary, then, a free parameter exists in the downstream solution which may be specified by a boundary condition there. This result supports the work by Forbes & Priest (1987) who examined the role of boundary conditions in both numerical and analytical models of reconnection. From a consideration of the characteristic slow-wave paths they also concluded that there is a free parameter downstream (see also Soward & Priest (1977) for an analysis of the characteristics). This essential result is unchanged by the inclusion of the effects of compressibility (see Chapter 5). In the compressible case, there is an extra jump relation which is obtained from the energy equation (which reduces to the mechanical energy equation or momentum equation in the incompressible limit). The inclusion, however, of density as an extra variable means that there is still one undetermined free parameter downstream.

This is an extremely important point to bear in mind when interpreting numerical models of reconnection, since the result may be strongly influenced by an imposed downstream boundary condition, such as the specification of the normal velocity at the outflow. Using a diffusion region model developed by Sonnerup (1988) we shall show in Chapter 3 that the free parameter may be prescribed by the velocity of plasma leaving the diffusion region (see also Jardine & Priest, 1988b). If, therefore, as in the numerical reconnection experiments of Biskamp (1986), the normal velocity is also prescribed at the downstream outflow boundary, this will cause a mismatch in velocities at the diffusion region and hence a region of reverse current. Indeed, Forbes & Priest (1987) have shown that many features of Biskamp's experiments can be understood in terms of their unified reconnection models, so that his claim to have disproved Petschek's mechanism is false; rather, Petschek's model is one of a much larger family of models. An important issue which is beyond the scope of

the present work is the temporal development of reconnection, for which numerical experiments are invaluable: for example Ugai (1987) has shown how fast steady reconnection can develop in response to a localised enhancement of resistivity.

2.6 Summary

In this chapter we have extended the Priest & Forbes (1986) family of models of reconnection to the next order in the expansion parameter. Attached to the diffusion region in these models is a discrete slow-mode compression in each quadrant which divides the region of interest into an upstream and a downstream part (See Figures 1.3 and 2.1). In the upstream region the different members of the family, characterized by a parameter b_0, can have markedly different configurations, from a slow-mode compression ($b_0 < 0$) with a converging flow to a flux pile-up regime ($b_0 > 1$) with a diverging flow. While to lowest order the downstream region is insensitive to the value of b_0, taking the next-order contribution has demonstrated that in fact a more general family of solutions exists downstream for each of the Priest & Forbes solutions.

To first order, the downstream configuration is of the form shown in Figure 2.2(a): the wave and the streamlines are straight and the field lines are curved. To second order, the wave is curved and the flow is converging. Both the pressure and the current density decrease with increasing x, but whereas the pressure is constant across the width of the region, the current density reaches a maximum on the wave (see Figure 2.5). As b_0 is increased through a slow compression to a flux pile-up regime, the magnitude of the downstream velocity increases linearly, the wave curvature increases and the width of the downstream region decreases. In contrast, the magnetic field, pressure and current density are, to the orders calculated here, unchanged; as indeed is the second-order y-component of velocity, which determines the degree of divergence of the flow.

Perhaps the most interesting feature to emerge has been the existence of a free parameter downstream. From an examination of the role played by the jump relations at the wave in relating the upstream and downstream solutions, we have shown that one boundary condition may be specified downstream. This result is extremely important in analytical or numerical models of reconnection, since they may be strongly influenced by the choice of this boundary condition.

CHAPTER 3

COMPARISON WITH NUMERICAL RESULTS

3.1 Introduction

Since the early models of Petschek and Sonnerup there have been several numerical experiments on reconnection. We will not attempt to review all of them here, but rather to describe a few as illustrative examples.

Quite recently, Biskamp (1982; 1984a,b; 1986) has published some numerical simulations which show features which would not be expected from previous models (see Figure 3.1). The inflow region is highly-nonuniform, the current sheet is long and thin and the outflow region is wide, with a very slow flow (approximately 0.2 v_{Ai} for the case $R_{me} = 873$ in Biskamp, 1986). At the outflow edges of the current sheet are small regions of reverse current (see Figure 3.1). Plasma flowing out of the diffusion region at approximately v_{Ai} appears to be deflected by these currents and flows instead in two fast jets along the separatrices (the magnetic field lines which pass through the neutral point). As M_e or R_{me} is increased, both the length and width of the diffusion region increase (which is exactly the opposite of what would be expected from Petschek's solution). Biskamp concluded from this that Petschek did not have a valid solution and suggested that the reason for this was that the diffusion region was not properly matched into the solution.

A rather different conclusion was reached by Lee & Fu. Their numerical experiments (Lee & Fu, 1986a,b and Fu & Lee, 1985) were similar to Biskamp's in that they found that the length of the diffusion region increases with M_e. They realised, however, that as M_e is increased, the nature of the inflow changes, from one having a fast-mode expansion to one having a slow-mode expansion. Using the way the dimensions of the diffusion region varied with M_e, Forbes & Priest (1987) were able to show that as M_e varied from 0.05 to 0.20, b_0 varied from -2 (slow-mode compression) to 4 (flux pile-up). They also examined Biskamp's results and showed that his scaling of the diffusion region with M_e or R_{me} could be explained by a progression through different reconnection regimes.

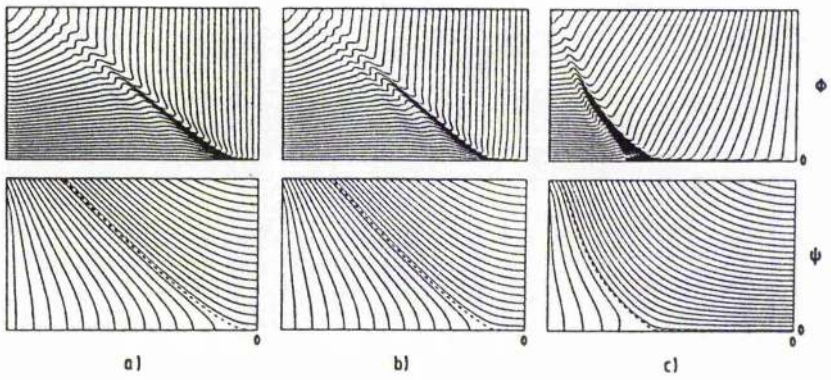

Figure 3.1: Streamlines (top) and field lines (bottom) from Biskamp (1986). Values of R_{me} are (a) 1746, (b) 3492 and (c) 6984.

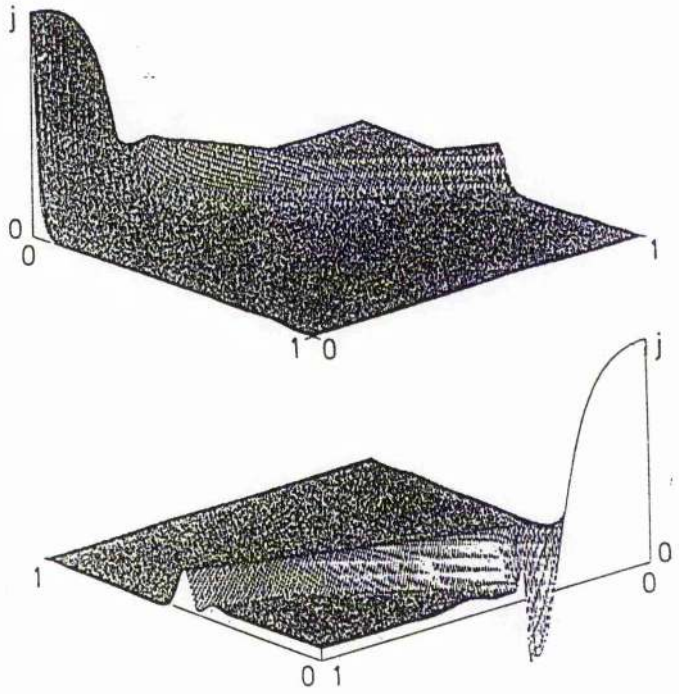

Figure 3.2: Current density plots from Biskamp (1986).
The current is concentrated in the diffusion region and the shock. Note also the region of reverse current near the diffusion region.

3.2 Reverse currents and separatrix jets

But what of the other unexpected features in Biskamp's work? Schindler & Birn (1987) suggested that the separatrix jets result from nonuniformities in the upstream field and a self-consistent model for them has been developed by Soward & Priest (1986) .The presence of reverse currents, on the other hand, (seen also in Forbes & Priest, 1982a; 1983a,b) can be explained in the light of the results of Chapter 2 (see also Jardine and Priest, 1988a). It was shown there that in the downstream region there is a free parameter, for example the x-component of velocity, which can be specified as a boundary condition. The velocity of plasma leaving the diffusion region is, however, determined by the *inflow* parameters and so this would seem naturally to determine the one unknown downstream. If, as in the work by Biskamp and Forbes & Priest, the velocity is also specified at the outflow boundary $|x| = 1$ of the downstream region, there will, in general, be a mismatch in velocity at the exit to the diffusion region (and therefore, from $\boldsymbol{E} = -\boldsymbol{v} \times \boldsymbol{B}$, a jump in the magnetic field strength there) which will give a current spike.

3.3 The effects of a velocity mismatch

In order to find some qualitative estimate of what the effects of specifying such a boundary condition would be on the coupled models of Chapter 2, we first need a better model of the diffusion region. One approach is to use a series expansion method (see also Biskamp 1986 and Sonnerup 1988) .

As an example to demonstrate the method, we could try expanding the resistive MHD equations as

$$\begin{aligned} \overline{A} &= a_0(\overline{x}) + a_2(\overline{x})\overline{y}^2 + a_4(\overline{x})\overline{y}^4 + \cdots \\ \overline{\Psi} &= b_1(\overline{x})\overline{y} + b_3(\overline{x})\overline{y}^3 + b_5(\overline{x})\overline{y}^5 + \cdots \end{aligned}$$

where A and Ψ are the flux function and stream function, respectively, such that $\boldsymbol{B} = \nabla A \times \hat{z}$ and $\boldsymbol{v} = \nabla\Psi \times \hat{z}$. We also nondimensionalise in the usual notation as $\overline{y} = y/\ell$, $\overline{x} = x/L$, $\overline{B} = B/B_i$, $\overline{v} = v/v_i$, $\overline{\Psi} = \Psi/V_iL$, $\overline{A} = A/B_iL$.

The three lowest powers of y (y^0, y^1 and y^2) then give, respectively:

$$1 - a_0'' M_i^2 - 2a_2 - a_0' b_1 = 0 \tag{3.1}$$

$$b_1(M_i^2 b_1''' + 6b_3') - b_1'(M_i^2 b_1'' + 6b_3)$$

$$-2a_2(M_i^2 a_0''' + 2a_2') + a_0'(2M_i^2 a_2'' + 24a_4) = 0 \tag{3.2}$$

$$2a_2 b_1 - M_i^2 a_2'' - 12a_4 - a_2' b_1 - 3a_0 b_3 = 0 \tag{3.3}$$

where we note that (3.2) may be rewritten using (3.1) and (3.3) as

$$b_3' - \left\{\frac{b_1' + (a_0')^2}{b_1}\right\} b_3 = \frac{1}{6}\left\{\left[-b_1''' + \frac{b_1' b_1''}{b_1} + (a_0'')^2 + 3a_0' a_0'' \frac{b_1'}{b_1} - a_0' a_0'''\right] M_i^2 \right.$$

$$\left. -2a_0' \frac{b_1'}{b_1} + 2(a_0')^2 b_1' - a_0'' - \frac{a_0' b_1'}{b_1}\right\} \tag{3.4}$$

Thus if, for example, a_0 and b_1 are chosen, these three equations will determine a_2, a_4 and b_3. Thereafter, each higher power will determine another unknown. The choice of these two coefficients is dictated by the facts that they must be of a sufficiently simple form that the integrating factor in (3.4) can be evaluated and also that, since

$$\begin{aligned}
\overline{B}_y &= -M_i\left(a_0' + a_2'\overline{y}^2 + a_4'\overline{y}^4 + \cdots\right) \\
\overline{B}_x &= 2a_2\overline{y} + 4a_4\overline{y}^3 + \cdots \\
\overline{v}_y &= -\left(b_1'\overline{y} + b_3'\overline{y}^3 + \cdots\right) \\
\overline{v}_x &= -\frac{1}{M_i}\left(b_1 + 3b_3\overline{y}^2 + \cdots\right)
\end{aligned}$$

we know that

1. v_x is odd in x, even in y
2. B_y is odd in x, even in y
3. v_y is even in x, odd in y
4. B_x is even in x, odd in y

With $a_0' = b_1 = -\tanh\overline{x}$ we then have

$$\begin{aligned}
\overline{v}_x &= \frac{1}{M_i}\left(-\tanh(\overline{x}) + 3b_3\overline{y}^2 + \cdots\right) \\
\overline{v}_y &= \operatorname{sech}^2(\overline{x})\overline{y} - b_3'\overline{y}^3 + \cdots \\
\overline{B}_x &= (1 + M_i^2)\operatorname{sech}^2(\overline{x})\overline{y} + 4a_4\overline{y}^3 + \cdots \\
\overline{B}_y &= M_i\left(\tanh(\overline{x}) + (1 + M_i^2)\operatorname{sech}^2(\overline{x})\tanh(\overline{x})\overline{y}^2 - a_4'\overline{y}^4 + \cdots\right)
\end{aligned}$$

where

$$a_4 = \frac{1}{12}(1+M_1^2)\mathrm{sech}^2(\overline{x})\left\{M_i^2\left[1-3\tanh^2(\overline{x})\right]-1\right\}+\frac{1}{4}\tanh(\overline{x})b_3$$
$$b_3 = \frac{2}{3}\tanh(\overline{x})\mathrm{sech}(\overline{x})\ln\left|\tanh\left(\frac{\overline{x}}{2}\right)\right|+\frac{1}{3}\tanh(\overline{x})\mathrm{sech}^2(\overline{x})+K\tanh(\overline{x})\mathrm{sech}(\overline{x})$$

and K is a constant.

This would then give the velocity and magnetic field strength within the diffusion region as functions of x and y. The problem with this particular example is that as $x \to 0$, $b_3' \to \infty$. It does, however, demonstrate the kind of approach which could be used. Using the results of Appendix A a downstream solution for a finite diffusion region could then be found.

The solutions we have available, however, are for cases where the length of the diffusion region is of the order of M_e (see Chapter 2) and so the variation across the width of the diffusion region may (for these models) be neglected. Taking, then, the outflow velocity to be just its value on the axis (v_{Ai}), we can see that since the electric field is constant, a mismatch in the axial value of v_x will be associated with a mismatch in B_y. Thus, B_y must change within, essentially, a diffusion length, η/v. For a velocity v_{Ai}, a global scale length L_e, a magnetic Reynolds number $R_{me} = v_{Ae}L_e/\eta$ and a diffusion region length $L = L_e/R_{me}M_e^{1/2}M_i^{3/2}$, this is just, to lowest order, $\delta x = (M_eL_e)^3$ (where we have followed the analysis of Chapter 2 in selecting the case $L/L_e = O(M_e)$). Hence, by Ampère's law, the current produced is

$$\mu j = O\left[\frac{\delta B_y}{(M_eL_e)^3}-\frac{\delta B_x}{M_eL_e}\right]\hat{z}. \tag{3.5}$$

In particular, since $B_{2y} = -(\mu\rho)^{1/2}M_ev_{1x}$, a mismatch in v_{1x} would give a current

$$\mu j = O\left[-(\mu\rho)^{1/2}\frac{\delta v_{1x}}{M_e^2L_e^3}\right]\hat{z}. \tag{3.6}$$

Now, the current within the diffusion region is approximately

$$\mu j = \left[-\frac{\partial B_x}{\partial y}\right]\hat{z} \tag{3.7}$$

and so if $\delta v_{1x} > 0$ a mismatch in velocity will give rise to a current opposite in direction to that within the diffusion region. Obviously, this approach cannot give quantitative predictions for the highly nonlinear regime of the numerical experiments. The essential result remains valid, however: that the specification of the normal velocity at the outflow will lead to a mismatch and hence a reverse current at the diffusion region.

CHAPTER 4

GLOBAL ENERGETICS OF FAST MAGNETIC RECONNECTION

4.1 Introduction

Now that we have a global family of reconnection models, one of the most interesting aspects of them to explore is the way that energy is transferred in the reconnection process. We would expect that the energy of the inflowing magnetic field would be converted into the kinetic and thermal energy of the outflow jet, but the details of this process are unclear. In examining the energetics of these solutions, we will show how the energy conversion differs betweeen the various reconnection regimes and explore the contribution of the wave to the energy conversion.

4.2 Energy transfer

In an incompressible, steady-state plasma, conservation of energy may be expressed as

$$\nabla . \left[(p + \tfrac{1}{2}\rho v^2)\boldsymbol{v} + \frac{\boldsymbol{E} \times \boldsymbol{B}}{\mu} \right] = 0. \tag{4.1}$$

Integrating this over a volume and using Gauss' theorem gives, in the two-dimensional case,

$$\int_B^C \left[(p + \tfrac{1}{2}\rho v^2)v_y + \frac{EB_x}{\mu} \right] dx = - \int_D^C \left[(p + \tfrac{1}{2}\rho v^2)v_x - \frac{EB_y}{\mu} \right] dy, \tag{4.2}$$

which simply states that the total amount of energy which flows into the region through the upper boundary (BC in Figure 4.1) must be equal to that which flows out of the side (CD).The first term on either side represents the thermal energy, the second the kinetic energy and the third the magnetic energy.

If we now dimensionalise as

$$p = \overline{p}p_e, \; v = \overline{v}v_e, \; B = \overline{B}B_e$$

with

$$E = v_e B_e$$

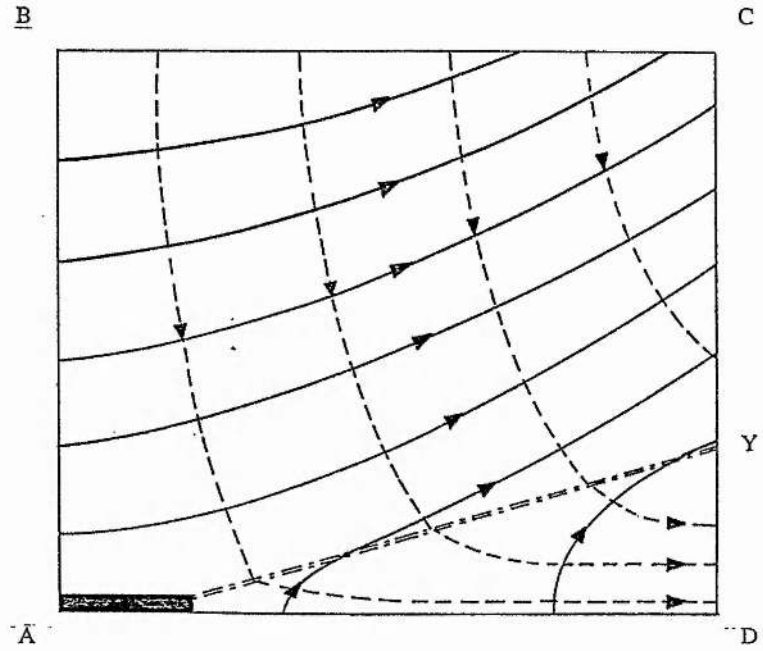

Figure 4.1: Schematic diagram of one quadrant of the reconnection model.

and expand both(4.2) and the length DY in powers of M_e, such that, for example,

$$Y = Y_0 + \epsilon Y_1 + \epsilon^2 Y_2 + \ldots$$

where ϵ is a small parameter of order M_e and

$$\frac{Y_1}{Y_0} = O(1),\ \frac{Y_2}{Y_1} = O(1),\ \text{etc.}$$

we obtain, after splitting the side boundary into two parts,

O(ϵ):

$$(\beta_e)_{\rm th} + (2)_{\rm mag} \;=\; [(1+\beta_e)_{\rm th} + (1)_{\rm kin}] \tag{4.3}$$

O(ϵ^2):

$$\begin{aligned}
&\int_0^1 \left[\beta_e\left(\tfrac{-\overline{v}_{2y}}{M_e} + \overline{p}_1\right)_{\rm th} + (2\overline{B}_{1x})_{\rm mag}\right] dx \\
&= -\int_0^C \left[\left(-\beta_e \tfrac{\overline{v}_{2x}}{M_e}\right)_{\rm th} - (2\overline{B}_{1y_{\rm mag}}\right] dy \\
&\quad + \frac{1}{M_e}\int_0^{Y_1} \left[\left((1+\beta_e)\overline{v}_{1x} + \tfrac{\beta_e \overline{p}_1}{M_e}\right)_{\rm th} + (3\overline{v}_{1x})_{\rm mag}\right] dy \\
&\quad + \frac{Y_2}{M_e}[(1+\beta_e)_{\rm th} + (1)_{\rm kin}]
\end{aligned} \tag{4.4}$$

(where we note that a term in $v_e B_e^2/2\mu$ has been cancelled on both sides). The subscripts 'th', 'kin' and 'mag' label the thermal, kinetic and magnetic contributions.

We note here that we have chosen to study only cases with $L \ll O(M_e)$ i.e. $\ell \ll O(M_e^2)$. The reason for this is that, as shown in Appendix A, some of the characteristics of the downstream solution propagate out from the diffusion region into the downstream region. Thus, if the diffusion region is of significant dimensions, then some part of the downstream region is traversed by these characteristics and so the solution for the whole of the downstream region can only be known if there is a full solution for the diffusion region. Given that this is not available, we choose to make the diffusion region small. This ensures that the 'region of influence' of the diffusion region is also small. In fact, this 'region of influence' of the diffusion region corresponds to the finite thickness of the wave, which we have neglected. The problem arises if we attempt to match a diffusion region of finite width to a wave of negligible width; this matching is only possible if we also neglect the width of the diffusion region.

Equations (4.3) and (4.4) express the global energy conservation of the system. The terms on the left-hand side represent energy flowing into the system through the upper boundary, while the terms on the right-hand side represent a flow of energy in or out through the side boundary. In (4.3), then, thermal and magnetic energy enter through the upstream (top) boundary, while thermal and kinetic energy leave through the downstream side boundary; there is no contribution from the upstream side boundary. To this order, then, the energetics of the system are fairly simple: the magnetic energy of the upstream region is converted in equal parts into the thermal and kinetic energy of the downstream flow. We note that all of this energy conversion takes place at the wave; there is no energy conversion within either the upstream or the downstream region. To this order, the total amount of energy flowing into the upstream region is

$$\int_0^1 \left[(p + \tfrac{1}{2}\rho v^2) v_y + \frac{E B_x}{\mu} \right] dx$$

and the ratio of thermal to kinetic energy flowing out of the downstream region is

$$\frac{\int_0^Y p v_x \, dy}{\int_0^Y \tfrac{1}{2}\rho v^2 v_x \, dy}$$

While the total amount of energy converted depends on the rate at which plasma is introduced into the system (essentially v_e) and on the value of the external plasma beta (β_e). the ratio of thermal to kinetic energy produced in the downstream region depends only on β_e. The value of b_0, which characterises the type of upstream solution, has no effect on the energetics at first order.

At second order the situation is a little more complex. As can be seen from (1.15). (1.18)

and (1.19) the left-hand side is zero, indicating that to this order there is no extra energy flow through the upper boundary, while the terms on the right-hand side depend not only on β_e and M_e, but also on b_0. The way in which the energy conversion depends on the reconnection regime can best be understood by considering the upstream and downstream regions separately. In the upstream region the balance of energy flowing through the side and through the wave respectively can be expressed as

$$\int_0^1 \left[\left(-\beta_e \frac{\overline{v}^u_{2x}}{M_e}\right)_{\rm th} - (2\overline{B}^u_{1y})_{\rm mag}\right] dy = -\int_0^1 \left[\beta_e\left(\frac{\overline{v}^u_{2y}}{M_e} - \overline{p}^u_1\right)_{\rm th} - (2\overline{B}^u_{1x})_{\rm mag}\right] dx$$

where the right-hand side is evaluated at $y = 0$. This may be rewritten using (1.15) to (1.20) as

$$\begin{aligned}
&\frac{4M_e}{L}\sum_{n=0}^{\infty}\frac{\tanh[(n+\frac{1}{2})\pi]}{[(n+\frac{1}{2})\pi]^2}\sin[(n+\tfrac{1}{2})\pi L] \\
&\times\left\{\beta_e\left(-b_0+\frac{\sin[(n+\frac{1}{2})\pi]}{(n+\frac{1}{2})\pi}\right)_{\rm th} - \left(\frac{2\sin[(n+\frac{1}{2})\pi]}{(n+\frac{1}{2})\pi}\right)_{\rm mag}\right\} \\
= \;& \frac{4M_e}{L}\sum_{n=0}^{\infty}\frac{\tanh[(n+\frac{1}{2})\pi]}{[(n+\frac{1}{2})\pi]^2}\sin[(n+\tfrac{1}{2})\pi L] \\
&\times\left\{\left((2+\beta_e)b_0-\beta_e\frac{\sin[(n+\frac{1}{2})\pi]}{(n+\frac{1}{2})\pi}\right)_{\rm th} + \left(-2b_0+\frac{2\sin[(n+\frac{1}{2})\pi]}{(n+\frac{1}{2})\pi}\right)_{\rm mag}\right\} \qquad (4.5)
\end{aligned}$$

When b_0 is negative there is a slow compression upstream such that the flow is strongly converging and the magnetic field strength decreases towards the diffusion region. Correspondingly, from (4.5), the thermal energy increases and the magnetic energy decreases as plasma flows through the region. As b_0 is increased beyond zero into the slow expansion regimes (for example, the flux pile-up regime, where the flow is strongly diverging and the magnetic field strength increases towards the diffusion region) there is a decrease in thermal energy and an increase in the magnetic energy of the plasma as it flows through the region. Thus to this order while the amount of energy flowing out of this region depends (from (4.5)) on M_e, β_e and b_0, the ratio of thermal to magnetic energy depends only on β_e.

Across the wave, conservation of energy requires that

$$\begin{aligned}
&\int_0^1 \left[\beta_e\left(-\frac{\overline{v}^u_{2y}}{M_e}+\overline{p}^u_1\right)_{\rm th} + \left(2\overline{B}^u_{1x}\right)_{\rm mag}\right] dx \\
&= \int_0^1 \Big[\left((1-\beta_e)\overline{B}^u_{1x}+\beta_e\overline{p}^u_1\right)_{\rm th} \\
&\quad +\left(2\overline{B}^u_{1x}(0)-\overline{B}^u_{1x}\right)_{\rm kin} \\
&\quad +2\left(\overline{B}^u_{1x}-\overline{B}^u_{1x}(0)\right)_{\rm mag}\Big] dx
\end{aligned}$$

(where superscripts u and d refer to upstream and downstream quantities respectively) or, using the results of (1.15) to (2.40)

$$\begin{aligned}
&\frac{4M_e}{L}\sum_{n=0}^{\infty}\frac{\tanh[(n+\frac{1}{2})\pi]}{[(n+\frac{1}{2})\pi]^2}\sin[(n+\tfrac{1}{2})\pi L]\\
&\times\left\{-\left((2+\beta_e)b_0-\beta_e\frac{\sin(n+\frac{1}{2})\pi}{(n+\frac{1}{2})\pi}\right)_{\rm th}+\left(2b_0-2\frac{\sin(n+\frac{1}{2})\pi}{(n+\frac{1}{2})\pi}\right)_{\rm mag}\right\}\\
=\;&-\frac{4M_e}{L}\sum_{n=0}^{\infty}\frac{\tanh[(n+\frac{1}{2})\pi]}{[(n+\frac{1}{2})\pi]^2}\sin[(n+\tfrac{1}{2})\pi L]\\
&\times\left\{\left((1+\beta_e)b_0+(1-\beta_e)\frac{\sin(n+\frac{1}{2})\pi}{(n+\frac{1}{2})\pi}\right)_{\rm th}-\left(b_0-2+\frac{\sin(n+\frac{1}{2})\pi}{(n+\frac{1}{2})\pi}\right)_{\rm kin}\right.\\
&\left.-\left(2-2\frac{\sin(n+\frac{1}{2})\pi}{(n+\frac{1}{2})\pi}\right)_{\rm mag}\right\}. \qquad (4.6)
\end{aligned}$$

Here, the form of the upstream solution affects the energy conversion mostly through the size and magnitude of the tangential component of the magnetic field (to this order, essentially B_{1x}). Thus if

$$\frac{4M_e}{L}\sum_{n=0}^{\infty}\frac{\tanh[(n+\frac{1}{2})\pi]}{[(n+\frac{1}{2})\pi]^2}\sin[(n+\tfrac{1}{2})\pi L]\left\{b_0-\frac{\sin(n+\frac{1}{2})\pi}{(n+\frac{1}{2})\pi}\right\}<0 \qquad (>0)$$

the thermal energy will decrease (increase); if

$$\frac{4M_e}{L}\sum_{n=0}^{\infty}\frac{\tanh[(n+\frac{1}{2})\pi]}{[(n+\frac{1}{2})\pi]^2}\sin[(n+\tfrac{1}{2})\pi L]\left\{b_0-2+\frac{\sin(n+\frac{1}{2})\pi}{(n+\frac{1}{2})\pi}\right\}<0 \qquad (>0)$$

the kinetic energy will decrease (increase) and if

$$\frac{4M_e}{L}\sum_{n=0}^{\infty}\frac{\tanh[(n+\frac{1}{2})\pi]}{[(n+\frac{1}{2})\pi]^2}\sin[(n+\tfrac{1}{2})\pi L]\left\{b_0-1+2\frac{\sin(n+\frac{1}{2})\pi}{(n+\frac{1}{2})\pi}\right\}>0 \qquad (<0)$$

the magnetic energy will decrease (increase).

Within the downstream region, the situation is slightly different, in that the energy conversion is independent of the form of the upstream solution. Conservation of energy may be written as

$$\begin{aligned}
&\int_0^1\left[\left((1-\beta_e)\overline{B}^u_{1x}+\beta_e\overline{p}^u_1\right)_{\rm th}+\left(2\overline{B}^u_{1x}(0)-\overline{B}^u_{1x}\right)_{\rm kin}+2\left(\overline{B}^u_{1x}-\overline{B}^u_{1x}(0)\right)_{\rm mag}\right]dx\\
=\;&\frac{1}{M_e}\int_0^1\left\{\left((1+\beta_e)\overline{v}^d_{1x}+\beta_e\overline{p}^d_1\right)_{\rm th}(3\overline{v}^d_{1x})_{\rm mag}\right\}dy+\frac{Y_2}{M_e}\left\{(1+\beta_e)_{\rm th}+(1)_{\rm kin}\right\}
\end{aligned}$$

or

$$\frac{4M_e}{L}\sum_{n=0}^{\infty}\frac{\tanh[(n+\frac{1}{2})\pi]}{[(n+\frac{1}{2})\pi]^2}\sin[(n+\frac{1}{2})\pi L]\left\{-\left((1+\beta_e)b_0+(1-\beta_e)\frac{\sin(n+\frac{1}{2})\pi}{(n+\frac{1}{2})\pi}\right)_{\rm th}\right.$$
$$\left.+\left(b_0-2+\frac{\sin(n+\frac{1}{2})\pi}{(n+\frac{1}{2})\pi}\right)_{\rm kin}+\left(2-2\frac{\sin(n+\frac{1}{2})\pi}{(n+\frac{1}{2})\pi}\right)_{\rm mag}\right\}$$
$$= -\frac{4M_e}{L}\sum_{n=0}^{\infty}\frac{\tanh[(n+\frac{1}{2})\pi]}{[(n+\frac{1}{2})\pi]^2}\sin[(n+\frac{1}{2})\pi L]\left\{\left((1+\beta_e)b_0-(1+\beta_e)\frac{\sin(n+\frac{1}{2})\pi}{(n+\frac{1}{2})\pi}\right)_{\rm th}\right.$$
$$\left.-\left(b_0-3\frac{\sin(n+\frac{1}{2})\pi}{(n+\frac{1}{2})\pi}\right)_{\rm kin}\right\}. \qquad (4.7)$$

Thus, to this order, the thermal energy and the kinetic energy increase at the expense of the magnetic energy which is released as the tension in the curved field lines accelerates plasma away from the diffusion region. Although the final ratio of thermal to kinetic energy which flows out of the downstream region depends on β_e, the change in energy which takes place within the downstream region is independent of either β_e, M_e or b_0.

If we now return to the energetics of the system as a whole and consider the sum of the $O(\epsilon)$ and $O(\epsilon^2)$ contributions together, we can see that the total amount of energy which flows into the upstream region (and is therefore available for conversion into other forms) increases as either M_e or β_e is increased and decreases on going from solutions with $b_0 < 0$ to those with $b_0 > 0$ (see Figure 4.2). This corresponds to a change from a strongly converging flow, which draws plasma in through the side boundary, to a strongly diverging flow, which pushes plasma out. Of the energy which flows out of the side boundary, the ratio of the (total) thermal to kinetic contributions i.e.

$$\frac{\int_0^Y p v_x\,dy}{\int_0^Y \frac{1}{2}\rho v^2 v_x\,dy}$$

also varies with b_0 (see Figure 4.3), decreasing linearly with b_0, such that, within the downstream region, thermal energy dominates for $b_0 \leq 0.3$ and kinetic energy dominates for $b_0 \geq 0.3$. As M_e is increased, and the size of the perturbed components increases, these variations with b_0 become much more pronounced; this behaviour is also seen in the variation of the total energy converted with b_0 (Figure 4.2). Finally, Figures 4.2 and 4.3 also show the variation of the downstream energy ratio and the total energy converted with β_e: an increase in β_e simply rescales these energies, without changing their intrinsic variation with b_0 or M_e.

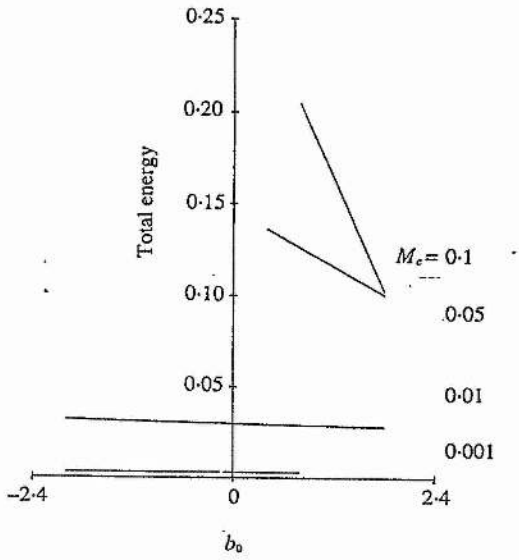

(a) $\beta_e = 1$

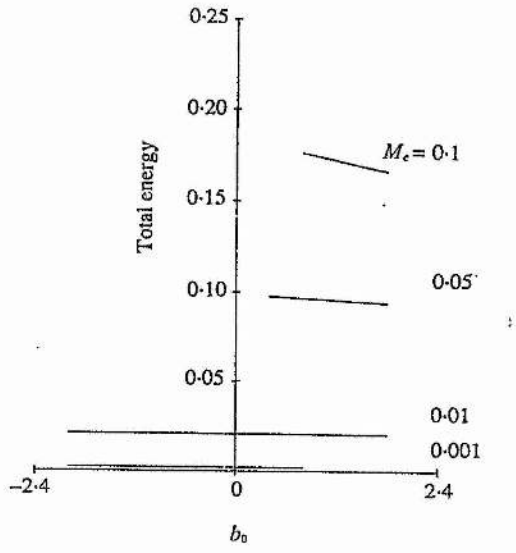

(b) $\beta_e = 0.1$

Figure 4.2: The variation of the total energy inflow with b_0 and the inflow Alfvén Mach number (M_e).

β_e is the upstream plasma beta.

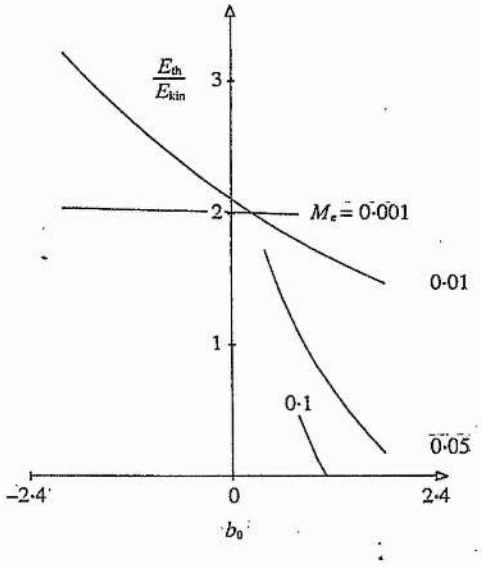

(a) $\beta_e = 1$

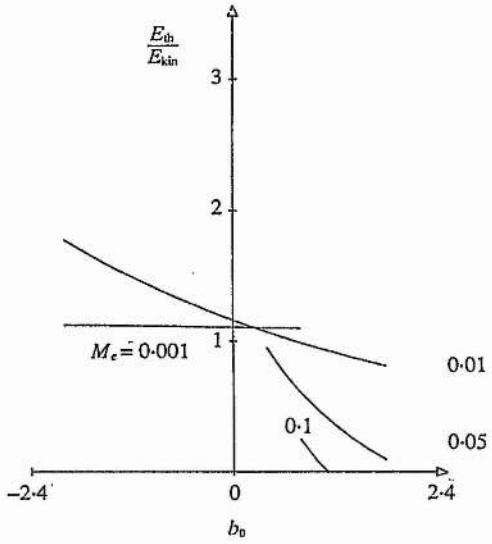

(b) $\beta_e = 0.1$

Figure 4.3: The variation of the ratio of thermal to kinetic energy downstream with b_0 and the inflow Alfvén Mach number (M_e).

4.3 Summary

We have examined the global energetics of the recent weakly nonlinear models for fast, steady state reconnection described in Chapter 2. This shows that, to first order, the energy conversion is insensitive to the type of solution (such as slow compression or flux pile-up), which is characterised by a parameter b_0. To the next order, however, both the amount of energy produced and the ratio of thermal to kinetic energy produced depends strongly on the type of solution. In addition, there is a dependence at both orders on the value of the external Mach number, M_e and the external plasma beta, β_e. These variations are such that in the region of accelerated plasma downstream of the wave, thermal energy dominates where M_e and β_e are large and the upstream flow is strongly converging, whereas kinetic energy will dominate where M_e is large, β_e is small and the upstream flow is strongly diverging. The total amount of energy converted is greatest when both M_e and β_e are large and the upstream flow is strongly converging.

CHAPTER 5

COMPRESSIBLE MODELS OF RECONNECTION

5.1 Introduction

In many reconnection models (including those just described in Chapters 1, 2) the assumption of incompressibility is used, partly because it can be the only way of rendering the problem tractable and partly because it is assumed that compressibility will not essentially affect the reconnection process. In reality, however, reconnection is often taking place in a fully compressible plasma (such as the solar corona) and so it is important to understand what the results of neglecting compressibility are.

In this chapter, we examine the effects of including compressibility on the global reconnection models of Chapters 1 and 2. We follow the analyses of these chapters closely in order that in the limit of $\gamma \to \infty$ we might recover the previous incompressible results. This allows us to assess the validity of the incompressible assumption in studying different aspects of the reconnection process and to show the modifications that are introduced when this assumption is relaxed.

5.2 The upstream region

We expand the MHD equations (1.1) to (1.5) for a compressible, steady-state plasma in powers of the inflow Mach number, M_e as described in Chapter 1. Expanding about a uniform density and magnetic field ($B_0 = B_{0x}\hat{x}$) and a stationary plasma ($v_0 = 0$) gives a solution of (1.1) to (1.5) for the magnetic field, electric current, plasma pressure, plasma velocity and density as:

$$\overline{B}_{1x} = \sum_{n=0}^{\infty} a_n \sinh\left[(n+\tfrac{1}{2})\pi(1-y)\right]\left\{b_n - \cos\left[(n+\tfrac{1}{2})\pi x\right]\right\},$$

$$\overline{B}_{1y} = \sum_{n=0}^{\infty} a_n \cosh\left[(n+\tfrac{1}{2})\pi(1-y)\right]\sin\left[(n+\tfrac{1}{2})\pi x\right],$$

$$\mu\overline{j}_1 = \sum_{n=0}^{\infty} a_n b_n (n+\tfrac{1}{2})\pi \cosh\left[(n+\tfrac{1}{2})\pi(1-y)\right],$$

$$\overline{p}_1 = -\frac{2}{\beta_e}\sum_{n=0}^{\infty} a_n b_n \sinh\left[(n+\tfrac{1}{2})\pi(1-y)\right],$$

$$\overline{v}_{2y} = M_e B_{1x},$$

$$\overline{v}_{2x} = -M_e\left[\overline{B}_{1y} - \left(1+\frac{v_{Ae}^2}{c_s^2}\right)\mu\overline{j}x\right], \tag{5.1}$$

$$\overline{\rho}_1 = \overline{\rho}_1^u - \frac{(\overline{p}_1 - \overline{p}_1^u)}{\gamma}. \tag{5.2}$$

where we have used dimensionless variables as described in Section 1.4. Note that the first five equations above are identical to (1.15) to (1.19) found by Priest & Forbes.

The boundary conditions used to obtain (1.15) to (1.19) and (5.1) to (5.2) are similar to those used by Priest & Forbes, i.e.

1. B_{1x} even in x (and therefore B_{1y} odd in x)
2. $\partial B_{1y}/\partial x = 0$ on $x = 1$
3. $B_{1x} = 0$ on $y = 1$
4. $B_{1y} = f(x)$ on $y = 0$

where

$$\begin{aligned} f(x) &= 2B_N && L \le x \le 1 \\ &= 2B_N x/L && 0 \le x \le L. \end{aligned}$$

$B_N = M_e B_e$ is the component of the magnetic field normal to the shock. This choice of $f(x)$ was made from considerations of the speed of the shocks; for the case of a compressible plasma we generalise this to $f(x) = \kappa B_N$ and obtain for the constant a_n:

$$a_n = \frac{2\kappa M_e \sin\left[(n+\frac{1}{2})\pi L\right]}{L(n+\frac{1}{2})^2\pi^2 \cosh\left[(n+\frac{1}{2})\pi\right]}. \tag{5.3}$$

As will be shown later, κ has a maximum value of 2 in the incompressible limit of $\gamma \to \infty$ and so the effect of introducing compressibility is to decrease a_n. Apart from this rescaling of a_n, however,equations (1.15) to (1.19) are identical to those found by Priest & Forbes. The main difference is in the perturbed transverse velocity, v_{2x}, which is enhanced by the factor $(1 + v_{Ae}^2/c_s^2)$. This factor tends to 1 as $c_s \to \infty$, so that in the incompressible limit we recover the Priest-Forbes solutions.

Since the density can now vary, the ratio of the magnetic field strength to the length of a field line need no longer be constant (since $\overline{B}/l = \overline{\rho}$) and so changes in the magnetic

field strength can be absorbed by density changes. This effect is most clearly seen in considering the hybrid regimes. In the incompressible case, as plasma flows in towards the diffusion region, the field strength decreases on the axis where the flow converges, but increases at the sides where the flow diverges. In the incompressible case, however, although the variations in the magnetic field are the same, they are no longer accompanied by the same changes in the direction of the flow.

The reason for this is the change in v_{2x}. Writing only the $n = 0$ contribution, (5.1) becomes

$$\overline{v}_{2x} = -M_e \left[a_n \frac{\pi}{2} \cosh\left[\frac{\pi}{2}(1-y)\right] \left\{ \sin\left[\frac{\pi}{2}x\right] - \left(1 + \frac{v_{Ae}^2}{c_s^2}\right) \frac{\pi}{2} b_0 x \right\} \right].$$

Thus, in the incompressible case ($(1 + v_{Ae}^2/c_s^2) \to 1$) we have the result that while, for $b_0 < 2/\pi$ the flow is purely converging and for $b_0 > 1$ it is purely diverging,for

$$\frac{2}{\pi} < b_0 < 1,$$

$\overline{v_{2x}}$ can change sign as x increases. The flow converges near the axis and diverges at the sides $|x| = 1$. In the compressible case, however, this condition becomes

$$\frac{2}{\pi}\left(1 + \frac{v_{Ae}^2}{c_s^2}\right)^{-1} < b_0 < \left(1 + \frac{v_{Ae}^2}{c_s^2}\right)^{-1}.$$

Hence, as the ratio v_{Ae}/c_s increases, the range of values of b_0 over which this hybrid behaviour occurs decreases, until, for $v_{Ae} \gg c_s$ (or $\beta \ll 1$), the flow is purely converging for the compressions ($b_0 < 0$) and purely diverging for the expansions ($b_0 > 0$). In this case, changes in the magnetic field strength are reflected in a change in the density structure and the flow pattern is more directly governed by variations in the plasma pressure.

One other consequence of the inclusion of compressibility is that it modifies the way in which the reconnection rate varies with the type of solution. This is traditionally measured by the external Alfvén Mach number M_e, which is simply the dimensionless rate at which field lines are carried towards the diffusion region for a given value of v_{Ae}. The particular choice of solution (or, equivalently, the choice of boundary conditions) will determine how the imposed flow is altered as it approaches the diffusion region, to give a local Mach number, M_i. As described in Chapter 1, Priest & Forbes showed that for each b_0 there is a unique relationship between M_e and M_i, such that, for example, for $b_0 < 1$, there is a maximum possible value of M_e. whereas for $b_0 > 1$ there is a maximum value of M_i.

This relationship is derived by considering that the electric field is uniform and hence

$$M_i = M_e \left(\frac{B_e}{B_i}\right)^2$$

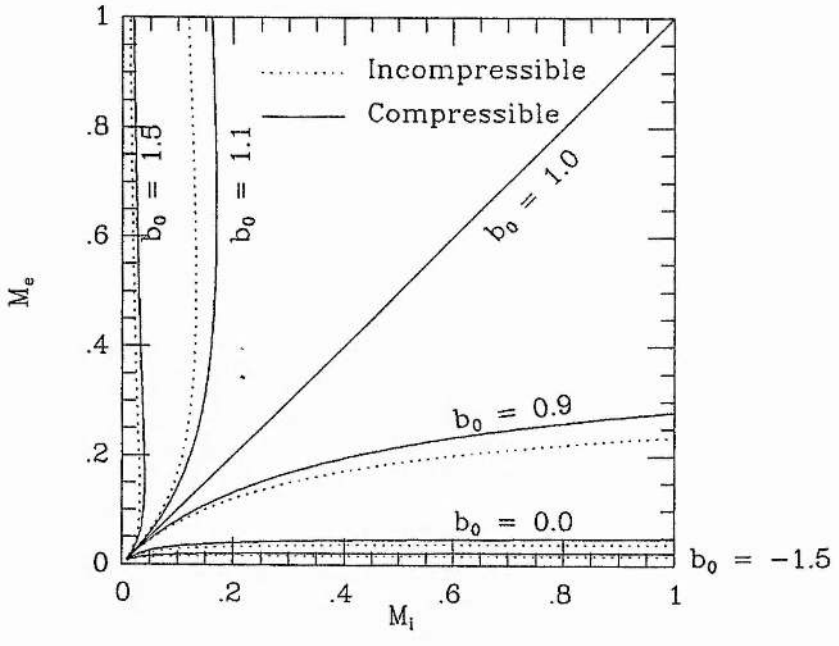

Figure 5.1: Reconnection rates in compressible and incompressible plasmas. The magnetic Reynolds number, R_{me}, is 5×10^7.

where B_i, the magnetic field strength at the diffusion region is given by Equation (1.22):

$$\begin{aligned} B_i &= B_e + B_{1x}(0,0) \\ &= B_e + \sum_{n=0}^{\infty} a_n(b_0 - 1)\sinh[(n+\tfrac{1}{2})\pi]. \end{aligned}$$

As shown by (5.3), however, the value of a_n is reduced in the compressible case and hence, from (1.22), the amount by which the field changes as it is carried towards the diffusion region is also reduced. Thus, for regimes with $b_0 > 1$ ($B_{1x} > 0$), the effect of introducing compressibility is to increase B_i and hence decrease M_i, while for $b_0 < 1$ the opposite is true. As can be seen from Figure 5.1, however, this is just a small correction and does not affect the overall behaviour of the reconnection rate.

5.3 The jump relations

The next step in finding a global solution is to look at the jump relations across the shock which forms the lower boundary of the upstream region. It is these jump relations which will be used to match the upstream and downstream solutions. Following Jeffrey and Taniuti (1964) , we write the jump relations for a compressible, two-dimensional steady-state plasma as

$$[\tau] = -\nu\langle\tau\rangle, \tag{5.4}$$

$$[v_n] = m[\tau], \tag{5.5}$$

$$[v_t] = \frac{B_n}{m\mu}[B_t], \tag{5.6}$$

$$[B_n] = 0, \tag{5.7}$$

$$[B_t] = \frac{-m^2[\tau]\langle B_t\rangle}{m^2\langle\tau\rangle - \frac{B_n^2}{\mu}}, \tag{5.8}$$

$$[p] = m[v_n] - \frac{1}{2\mu}[{B_t}^2], \tag{5.9}$$

$$\left[\frac{p}{\rho(\gamma-1)} + \langle p\rangle\tau\right] = -\frac{1}{4\mu}[\tau][B_t]^2, \tag{5.10}$$

where, as before, $[X] = X^d - X^u$, $\langle X\rangle = \frac{1}{2}(X^d + X^u)$ and ν characterises the jump in density. The mass flux is $m = \rho c_n$ where c_n is the characteristic wave speed and $\tau = 1/\rho$. Since the shock is stationary, we may write $m = \rho v_n$. These jump relations may then be rewritten as:

$$\rho^d = R\rho^u \tag{5.11}$$

$$v_n^d = \frac{v_n^u}{R} \tag{5.12}$$

$$v_t^d - v_t^u = \frac{B_n}{\mu\rho^u v_n^u}\left\{B_t^d - B_t^u\right\} \tag{5.13}$$

$$B_n^d = B_n^u \tag{5.14}$$

$$B_t^d = RB_t^u\frac{(v_n^u)^2 - (v_A^u)^2}{(v_n^u)^2 - R(v_A^u)^2} \tag{5.15}$$

$$p^d = p^u - \rho^u v_n^u(v_n^d - v_n^u) - \frac{1}{2\mu}\{(B_t^d)^2 - (B_t^u)^2\} \tag{5.16}$$

$$\frac{\rho^u\rho^d}{2}(p^u + p^d)(\rho^u - \rho^d) + \frac{\rho^u p^d}{\gamma-1} - \frac{\rho^d p^u}{\gamma-1} = \frac{\rho^d - \rho^u}{4\mu}[B_t]^2 \tag{5.17}$$

where the shock strength $R = (2+\nu)/(2-\nu)$.

As described in Jardine & Priest (1988a) and in Chapter 2, these may be expressed in terms of in x and y-components and expanded in powers of M_e. The resulting equations are most easily tackled by looking first at the lowest orders of each expansion. Thus, from (5.11):

$$O(1) \qquad \overline{\rho}_0^d = \overline{\rho}_0^u R_0 \tag{5.18}$$

$$O(\epsilon) \qquad \overline{\rho}_1^d = \overline{\rho}_1^u R_0 + R_1 \tag{5.19}$$

while from (5.16), with $\overline{B}^u_{1y} = \kappa M_e$ and $\tan\alpha_1 = \zeta M_e$ where α is the angle made by the tangent to the shock with the x-axis,

$$O(1) \qquad \tan\alpha_0 = 0 \tag{5.20}$$

$$O(\epsilon) \qquad (\kappa-\zeta)^2 = \frac{(1+R_0)\beta_e(\overline{p}^d_0-1)+(R_0-1)\{1+(\overline{B}^d_{0x})^2\}}{2R_0\beta_e(\overline{p}^d_0-1)} \tag{5.21}$$

and from (5.15)

$$O((1) \qquad \overline{B}^d_{0x} = R_0\frac{(1-(\kappa-\zeta)^2)}{(1-R_0(\kappa-\zeta)^2)}. \tag{5.22}$$

In order to be able to compare our results with those from the incompressible analysis, however, we must choose $B_{0x} = 0$ in the downstream region. Hence

$$\kappa - \zeta = 1 \tag{5.23}$$

and so (5.21) becomes

$$\overline{p}^d_0 = \frac{1+\beta_e}{\beta_e}. \tag{5.24}$$

Comparing this with (5.17):

$$O(1) \qquad \overline{p}^d_0 = \frac{\beta_e[2R_0-(1-R_0)(\gamma-1)]-(\gamma-1)(1-R_0)}{\beta_e[2+(1-R_0)(\gamma-1)]} \tag{5.25}$$

gives

$$R_0 = \frac{\gamma(\beta_e+1)}{\gamma(\beta_e+1)-1}. \tag{5.26}$$

We also have from (5.14)

$$O(1) \qquad \overline{B}^d_{0y} = 0 \tag{5.27}$$

$$O(\epsilon) \qquad \overline{B}^d_{1y} = M_e \tag{5.28}$$

and from (5.12)

$$O(1) \qquad \overline{v}^d_{0y} = 0 \tag{5.29}$$

$$O(\epsilon) \qquad \overline{v}^d_{1y} = -\frac{M_e}{R_0} + \overline{v}^d_{0x}\zeta M_e. \tag{5.30}$$

As we will show later, however, $\overline{v}_{1y} = 0$ in the downstream region and so, from (5.30)

$$\overline{v}^d_{0x} = \frac{1}{R_0\zeta}$$

but, from (5.13)

$$O(1) \qquad \overline{v}^d_{0x} = 1$$

and so

$$\zeta = \frac{1}{R_0}. \tag{5.31}$$

and

$$\kappa = 1 + \frac{1}{R_0} \tag{5.32}$$

Thus, in the limit $\gamma \to \infty$, we find $R_0 \to 1$ and $\kappa \to 2$ and so, as discussed before, κ has a maximum of 2 in the incompressible limit. With the results of (5.18) to (5.31) we can now simplify the higher orders in the expansions, such as, from (5.15)

$$O(\epsilon) \qquad \overline{B}^d_{1x} = \frac{R_0}{1-R_0}\left\{\overline{p}^u_1 - 2\overline{B}^u_{1x} - 2\left(\frac{\overline{B}^u_{2y}}{M_e} - \frac{\tan\alpha_2}{M_e} - \frac{\overline{B}^u_{1x}}{R_0}\right)\right\}. \tag{5.33}$$

Using this and (5.24) we find that the first-order contribution to (5.16) gives

$$\overline{p}^d_1 = \overline{p}^u_1 + \frac{2}{\beta_e}\overline{B}^u_{1x} \tag{5.34}$$

and comparing this with the first-order part of (5.17), i.e.

$$\begin{aligned}\overline{p}^d_1 \;=\; & \frac{1}{2+(1-R_0)(\gamma-1)}\Big\{\left[2\overline{\rho}^d_1 - (\overline{\rho}^u_1 - \overline{\rho}^d_1)(\gamma-1)\right] - \overline{p}^d_0\left[2\overline{\rho}^u_1 + (\overline{\rho}^u_1 - \overline{\rho}^d_1)(\gamma-1)\right]\cdot \\ & + \overline{p}^u_1\left[2R_0 - (1-R_0)(\gamma-1)\right] - \frac{(\gamma-1)}{\beta_e}\left[\overline{p}^u_1 - \overline{p}^d_1 + 2(1-R_0)(\overline{B}^u_{1x} - \overline{B}^d_{1x})\right]\Big\}\end{aligned}$$

gives, after some algebra,

$$\begin{aligned}\left(\frac{\overline{B}^u_{2y}}{M_e} - \frac{\tan\alpha_2}{M_e} - \frac{\overline{B}^u_{1x}}{R_0}\right) \;=\; & -\frac{\beta_e}{2}\frac{\gamma}{(\gamma-1)}\frac{(1-R_0)}{R_0}\overline{p}^u_1 \\ & -\frac{\gamma}{R_0(\gamma-1)}\overline{B}^u_{1x} + \frac{\overline{p}^u_1}{2} - \frac{R_1}{2R_0(1-R_0)(\gamma-1)}\end{aligned} \tag{5.35}$$

which, substituted into (5.33) gives

$$\overline{B}^d_{1x} = \frac{\gamma\beta_e}{\gamma-1}\left(\overline{p}^u_1 - 2\overline{B}^u_{1x}\right) + \frac{R_1}{(1-R_0)^2(\gamma-1)}. \tag{5.36}$$

Finally we have, from (5.14)

$$\overline{B}^d_{2y} = M_e\left[\left(\frac{\overline{B}^u_{2y}}{M_e} - \frac{\tan\alpha_2}{M_e} - \frac{\overline{B}^u_{1x}}{R_0}\right) + \frac{\overline{B}^d_{1x}}{R_0}\right], \tag{5.37}$$

from (5.12)

$$\overline{v}^d_{2y} = \frac{M_e}{R_0}\left(\frac{R_1}{R_0} + \overline{B}^u_{1x} + \overline{v}^d_{1x} + \frac{R_0}{M_e}\tan\alpha_2\right) \tag{5.38}$$

and from (5.18)

$$\overline{v}^d_{1x} = 2\overline{B}^u_{1x} - \overline{p}^u_1 - \overline{B}^d_{1x} + \left(\frac{\overline{B}^u_{2y}}{M_e} - \frac{\tan\alpha_2}{M_e} - \frac{\overline{B}^u_{1x}}{R_0}\right). \tag{5.39}$$

5.4 The downstream region

As in the upstream region, we expand (1.1) to (1.5) in powers of M_e about the same lowest order configuration as was used in the incompressible case. Thus we choose $\overline{v}_{0x} = 1$ and $\overline{B}_{0x} = 0$ with $\overline{p}_0^d = R_0$. Once again we rescale the y-coordinate as $y = \epsilon y'$ where ϵ is a small parameter of order M_e. Several results can be seen straight away from (1.2) and (5.27). Firstly,

$$B_{0y} = 0$$

while from (1.3), invoking symmetry,

$$v_{0y} = 0$$

and so from (1.2) again

$$\begin{aligned} \overline{B}_{1y} &= \text{const} \\ &= M_e \end{aligned}$$

from (5.28). Finally, from (1.5), (5.24) and (5.34)

$$\overline{p}_0 = \frac{1+\beta_e}{\beta_e}$$

and

$$\overline{p}_1 = \overline{p}_1^u + \frac{2}{\beta_e}\overline{B}_{1x}^u.$$

This leaves six equations, namely,

$$\frac{\partial \overline{B}_{1x}}{\partial x} + \frac{\partial \overline{B}_{2y}}{\partial y} = 0 \tag{5.40}$$

$$\overline{B}_{2y} + \overline{v}_{1x} M_e = 0 \tag{5.41}$$

$$\frac{\partial \overline{p}_1}{\partial x} + R_0 \left(\frac{\partial \overline{v}_{1x}}{\partial x} + \frac{\partial \overline{v}_{2y}}{\partial y} \right) = 0 \tag{5.42}$$

$$R_0 \frac{d\overline{p}_1}{dx} = \frac{\gamma(1+\beta_e)}{\beta_e} \frac{\partial \overline{\rho}_1}{\partial x} \tag{5.43}$$

$$R_0 \frac{\partial \overline{v}_{1x}}{\partial x} = -\frac{\beta_e}{2} \frac{d\overline{p}_1}{dx} + M_e \frac{\partial \overline{B}_{1x}}{\partial y} \tag{5.44}$$

$$\frac{\partial \overline{p}_2}{\partial y} = -\frac{2}{\beta_e} \overline{B}_{1x} \frac{\partial \overline{B}_{1x}}{\partial y} \tag{5.45}$$

Now, (5.40) and (5.41) give

$$\frac{\partial \overline{B}_{1x}}{\partial x} = M_e \frac{\partial \overline{v}_{1x}}{\partial y} \tag{5.46}$$

which, with (5.44) gives

$$\frac{\partial^2 \overline{B}_{1x}}{\partial x^2} - \frac{M_e^2}{R_0} \frac{\partial^2 \overline{B}_{1x}}{\partial y^2} = 0 \tag{5.47}$$

which has the general solution

$$B_{1x} = f(y + \frac{M_e}{R_0^{1/2}}x) + g(y - \frac{M_e}{R_0^{1/2}}x)$$

where f and g are arbitrary functions. Using the boundary conditions

$B_{1x} = 0$ on $y = 0$

$B_{1x} = B_{1x}^d$ on $y = \frac{M_e}{R_0}x$ (which, from (5.31) is the lowest-order wave position)

we obtain (see Appendix C for details)

$$\begin{aligned}\overline{B}_{1x} &= \sum_{q=0}^{\infty} \overline{B}_{1x}^d \left[\frac{\xi^q R_0}{M_e(1+R_0^{1/2})}(y + \frac{M_e}{R_0^{1/2}}x)\right] - \overline{B}_{1x}^d \left[\frac{\xi^q R_0}{M_e(1+R_0^{1/2})}(y - \frac{M_e}{R_0^{1/2}}x)\right] \\ &= \tfrac{1}{2}\Big\{R_0^{1/2}\left[\overline{v}_{1x}^d(c^+) - \overline{v}_{1x}^d(c^-)\right] + \left[\overline{B}_{1x}^d(c^+) - \overline{B}_{1x}^d(c^-)\right] \\ &\quad + \frac{\beta_e}{2R_0^{1/2}}\left[\overline{p}_1^d(c^+) - \overline{p}_1^d(c^-)\right]\Big\} \qquad (5.48)\end{aligned}$$

where

$$\begin{aligned}c^+ &= \frac{R_0(y + \frac{M_e}{R_0^{1/2}}x)}{M_e(1+R_0^{1/2})}, \\ c^- &= \frac{R_0(y - \frac{M_e}{R_0^{1/2}}x)}{M_e(1+R_0^{1/2})},\end{aligned}$$

and

$$\xi = \frac{R_0^{1/2} - 1}{R_0^{1/2} + 1}. \qquad (5.49)$$

Also, from (5.44) and (5.46) we obtain

$$\begin{aligned}\overline{v}_{1x} &= \frac{1}{2R_0^{1/2}}\Big\{R_0^{1/2}\left[\overline{v}_{1x}^d(c^+) + \overline{v}_{1x}^d(c^-)\right] + \left[\overline{B}_{1x}^d(c^+) + \overline{B}_{1x}^d(c^-)\right] \\ &\quad + \frac{\beta_e}{2R_0^{1/2}}\left[\overline{p}_1^d(c^+) + \overline{p}_1^d(c^-) - 2\overline{p}_1^d(x)\right]\Big\}. \qquad (5.50)\end{aligned}$$

Subtracting (5.48) from (5.50) and evaluating the resulting expression at the shock gives

$$\overline{v}_{1x}^d - \frac{\overline{B}_{1x}^d}{R_0^{1/2}} + \frac{\beta_e}{2R_0}\overline{p}_1^d = \overline{v}_{1x}^d(-\xi x) + \frac{\overline{B}_{1x}^d}{R_0^{1/2}}(-\xi x) + \frac{\beta_e}{2R_0}\overline{p}_1^d(-\xi x). \qquad (5.51)$$

This is a constraint which must be satisfied if the first-order upstream and downstream solutions are to match. If we use (5.39), (5.36) and (5.34) to substitute for $\overline{v}_{1x}^d$, $\overline{B}_{1x}^d$ and $\overline{p}_1^d$, we can write (5.51) as

$$\begin{aligned}&(c_3 - c_2)R_1(x) + (c_3 + c_2)R_1(\xi x) = \\ &\quad \sum_{n=0}^{\infty} a_n \sinh\left[(n+\tfrac{1}{2})\pi\right]\Big\{-(c_0 + c_1)\cos\left[(n+\tfrac{1}{2})\pi x\right] \\ &\quad + (c_0 - c_1)\cos\left[(n+\tfrac{1}{2})\pi\xi x\right] - c_4 b_0\Big\}. \qquad (5.52)\end{aligned}$$

where

$$
\begin{aligned}
c_0 &= 2(1-R_0)^2\left[(1+R_0)(\gamma-1)-1+2R_0\gamma\beta_e\right] \\
c_1 &= 4(1-R_0)^2R_0^{1/2}\gamma\beta_e \\
c_2 &= (1-R_0)^2(\gamma-1)-(1+R_0) \\
c_3 &= 2R_0^{1/2} \\
c_4 &= 8R_0^{3/2}(1-R_0)
\end{aligned}
$$

(for the method used to solve this equation, see Appendix D).

Thus, it is the first-order matching of the two solutions which determines $R_1(x)$, the perturbation to the shock strength, just as it was essentially the choice of $B^d_{0x}=0$ which determined R_0. As one would expect, the shock strength simply adjusts to accommodate the existing downstream solution.

Now that v_{1x} and B_{1x} have been found, the other unknowns of the downstream solution follow easily. From (5.42) and (5.43)

$$\frac{\partial \overline{v}_{2y}}{\partial y} = -\frac{\partial \overline{v}_{1x}}{\partial x} - \frac{\beta_e}{\gamma(\beta_e+1)}\frac{d\overline{p}^d_1}{dx} \tag{5.53}$$

which, using (5.44) and the fact that $\overline{v}_{2y}=0$ on $y=0$, gives

$$\overline{v}_{2y} = \frac{\beta_e}{2R_0}(3-2R_0)\frac{d\overline{p}^d_1}{dx}y - \frac{M_e}{R_0}\overline{B}_{1x}. \tag{5.54}$$

This now allows us to find the second-order shock position, since evaluating (5.54) at the shock and eliminating $\overline{v}^d_{2y}$ from (5.54) and (5.38) gives

$$\frac{R_0}{M_e}\tan\alpha_2 = \frac{\beta_e}{2R_0}(3-2R_0)x\frac{d\overline{p}^d_1}{dx} - \left(\frac{R_1}{R_0}+\overline{v}^d_{1x}+\overline{B}^u_{1x}+\overline{B}^d_{1x}\right). \tag{5.55}$$

Since $\alpha_2 = dy_2/dx$, integrating (5.55) gives

$$
\begin{aligned}
y_2 = \frac{M_e}{R_0^2(\gamma-1)}\Bigg\{&\left[\frac{1-3(1-R_0)(\gamma-1)}{2(1-R_0)}\right]\int_0^x R_1(x)\,dx + \sum_{n=0}^{\infty} a_n \sinh\left[(n+\tfrac{1}{2})\pi\right] \\
&\times\Bigg[(3-2\gamma)R_0b_0x - (3-2R_0)(\gamma-1)x\cos\left[(n+\tfrac{1}{2})\pi x\right] \\
&+(3\gamma-4)\frac{\sin\left[(n+\tfrac{1}{2})\pi x\right]}{(n+\tfrac{1}{2})\pi}\Bigg]\Bigg\}.
\end{aligned} \tag{5.56}
$$

In addition, the first-order density can be found from (5.43), assuming that $\overline{\rho}_1(1)=0$:

$$\overline{\rho}_1 = (R_0-1)\beta_e\overline{p}^d_1 \tag{5.57}$$

and thus, from (5.19)

$$\overline{\rho}_1^u = \frac{(R_0 - 1)\beta_e \overline{p}_1^d - R_1}{R_0} \tag{5.58}$$

and from (5.2) the *upstream* density becomes

$$\overline{\rho}_1 = \frac{(R_0 - 1)\beta_e \overline{p}_1^d - R_1}{R_0} - \frac{\overline{p}_1 - \overline{p}_1^u}{\gamma}. \tag{5.59}$$

Equations (5.40) and (5.41) also give

$$\overline{B}_{2y} = \overline{B}_{2y}^d + M_e(\overline{v}_{1x} - \overline{v}_{1x}^d) \tag{5.60}$$

and from (5.45)

$$\overline{p}_2 = \overline{p}_2^d - \frac{(\overline{B}_{1x})^2 - (\overline{B}_{1x}^d)^2}{\beta_e}. \tag{5.61}$$

Finally, the current density can be found from the solution for B_{1x}, since, from

$$j = \frac{\nabla \times B}{\mu}$$

we have

$$j_0 = -\frac{\partial B_{1x}}{\partial y}$$

which, using (5.48), (5.39), (5.36) and (5.34) to give

$$\begin{aligned} B_{1x} \;=\; & \frac{1}{4(1-R_0)^2 R_0^{1/2}(\gamma-1)} \Big\{ (c_2 + c_3)\left[R_1(c^+) - R_1(c^-)\right] \\ & + (c_1 - c_0) \sum_{n=0}^{\infty} a_n \sinh\left[(n+\tfrac{1}{2})\pi\right] \Big(\cos\left[(n+\tfrac{1}{2})\pi c^+\right] \\ & - \cos\left[(n+\tfrac{1}{2})\pi c^-\right] \Big) \Big\} \end{aligned} \tag{5.62}$$

(using the notation of (5.53)), is just

$$\begin{aligned} j_0 \;=\; & -\frac{R_0^{1/2}}{4M_e(1-R_0)^2(1+R_0^{1/2})(\gamma-1)} \Big\{ (c_2 + c_3)\left[R_1'(c^+) - R_1'(c^-)\right] \\ & + (c_1 - c_0) \sum_{n=0}^{\infty} a_n (n+\tfrac{1}{2})\pi \sinh\left[(n+\tfrac{1}{2})\pi\right] \Big(\sin\left[(n+\tfrac{1}{2})\pi c^+\right] \\ & - \sin\left[(n+\tfrac{1}{2})\pi c^-\right] \Big) \Big\} \end{aligned} \tag{5.63}$$

We note here that since we have assumed a particular form for the downstream density variation (see equation (5.57)), we have already chosen the 'free parameter' mentioned in Chapter 2. There, the unknown parameter was determined by choosing v_{1x} such that there was a velocity match at the outflow of the diffusion region. Here, the choice of $\overline{\rho}_1(1) = 0$ is made in order to simplify the equations, but it will not ensure that such a

velocity match exists. This *could* be done by retaining the arbitrary function of y in (5.57) which was removed by the above assumption. Equation (5.50) for v_{1x} would then include this function of y through the expression for v_{1x}^d (5.50). If the variation of v_{1x} with y at the outflow boundary of the diffusion region were known, then this function could be evaluated and a velocity match would be ensured.

The fact that the free parameter has been specified in different ways in this and the previous chapter means that although the incompressible limit of the compressible solution should resemble the results of Chapter 2 in *character*, it will not be exactly the same.

5.5 The effects of compressibility

As was the case in the upstream region, the inclusion of compressibility does not affect the essential character of the downstream region. In fact, to first order, both the pressure and the y-components of the velocity and the magnetic field are unaltered (see also Semenov et al, 1983a for a comparison with the results for Petschek's model). The main reason for this is simply that the width of the downstream region is of the same order as the perturbation and so, at the lower orders, there is little variation across it.

The x-components of velocity and magnetic field strength do show some difference and of course there is now a density gradient in the x-direction, but the variation of the solutions with changes in the reconnection regime (or equally b_0) is not affected. The perturbed x-component of velocity v_{1x} still increases linearly with b_0 while both B_{1x} and v_{2y} show no explicit b_0 dependence. It is perhaps worth noting here, however, that there is some slight dependence of all parameters on b_0 due to the fact that the length of the diffusion region, L, which enters into the expression for each parameter, does vary with b_0. This is a very small effect, however, particularly where, as chosen here, $L << 1$. We also find that the lowest-order current density, j_0, is independent of b_0, while the second -order shock position, y_2 varies linearly with b_0. This is exactly what was found in the incompressible case.

The main effect, then of including compressibility is not to change the way that the solutions vary with the different reconnection regimes, but, within each regime, to affect how the magnetic field and the plasma interact. In the upstream region, introducing compressibility and therefore allowing changes in the magnetic field strength to change the density of the plasma, alters the way in which the magnetic field is able to influence the transverse velocity. In the downstream region, there is a similar situation. Here, the

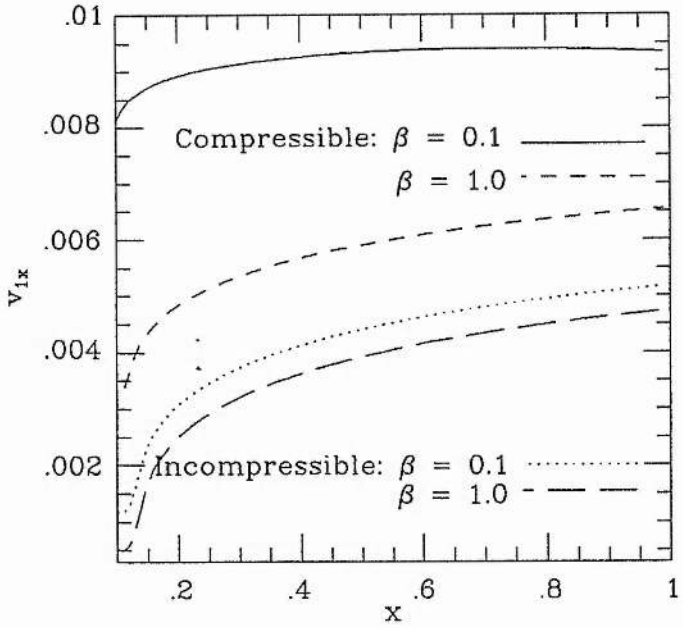

Figure 5.2: The perturbed x-component of the downstream velocity vs. x. Curves for different values of β_e are shown for the compressible and incompressible cases.

newly-reconnected field lines are highly curved and the tension in these field lines, which acts to reduce their curvature, accelerates plasma away from the diffusion region. As the field lines straighten out, they transfer some of their energy to the plasma, which is accelerated and heated.

If the plasma is incompressible, then the tension force cannot change the density of the plasma, only propel it. In this case the curvature of the field lines decreases more slowly than in the compressible case, where the fieldlines straighten out closer to the diffusion region and accelerate the plasma more effectively. This behaviour can be seen in Figures 5.2 and 5.3 which show how the perturbed x-components of velocity and magnetic field strength vary with distance from the diffusion region. Two different values of γ are chosen : $\gamma = 5/3$, representing a fully compressible plasma and $\gamma = 10$, representing an almost incompressible plasma. Figure 5.3 shows the variation of B_{1x} or, equally the field curvature, since B_{1y} is a constant. For both values of γ, the curvature decreases to almost zero away from the diffusion region ($x = 0$), but in the incompressible case this decrease is slower. The effect of changes in the field curvature can be seen in Figure 5.2 which shows a greater acceleration of the plasma near the diffusion region in the compressible case.

The absolute value of the x-components of velocity and magnetic field (as opposed to

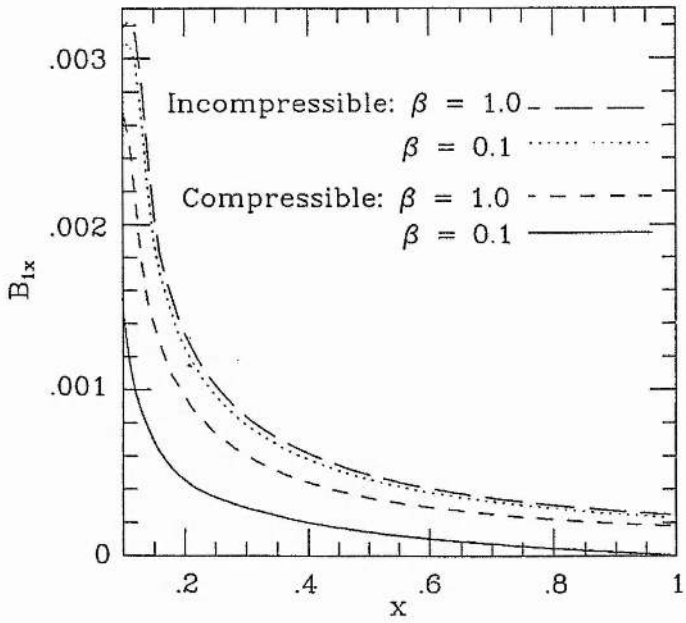

Figure 5.3: The perturbed x-component of the downstream magnetic field vs. x. Curves for different values of β_e are shown for the compressible and incompressible cases.

their variation with x) also differ in the compressible and incompressible cases. The reason for this is that from (5.26) the lowest-order shock strength R_0 is a function of γ such that in the limit $\gamma \to \infty$, $R_0 \to 1$. Thus in an incompressible plasma, the shock strength (and hence the jump in the transverse components of velocity and magnetic field strength) is reduced. Hence setting $\gamma \to \infty$ gives a larger value of B_{1x} downstream and a smaller value of v_{1x}.

The lowest-order current density is also slightly different in the two cases. In both, there are current maxima at the shocks and at the diffusion region, with a minimum on the x-axis. In the compressible case, however, where the field line curvature decreases rather more rapidly away from the diffusion region, the current density also reaches its minimum closer to $x = 0$. The plasma density, on the other hand, is very different in the two cases, since in the incompressible limit there is no density perturbation at all. For a compressible plasma, the total density varies as $1 - 2[(R_0 - 1)/R_0]\cos(\pi/2)x$ (taking only the first term in the summation in (5.57)). Thus, it increases from a minimum at $x = 0$ to a maximum at $x = 1$ as the tension force compresses the plasma.

The variation of the field curvature is also reflected in the variation of v_{2y} as in equation (5.54) and Figure 5.4, being largest where the field strength is largest. The same is also

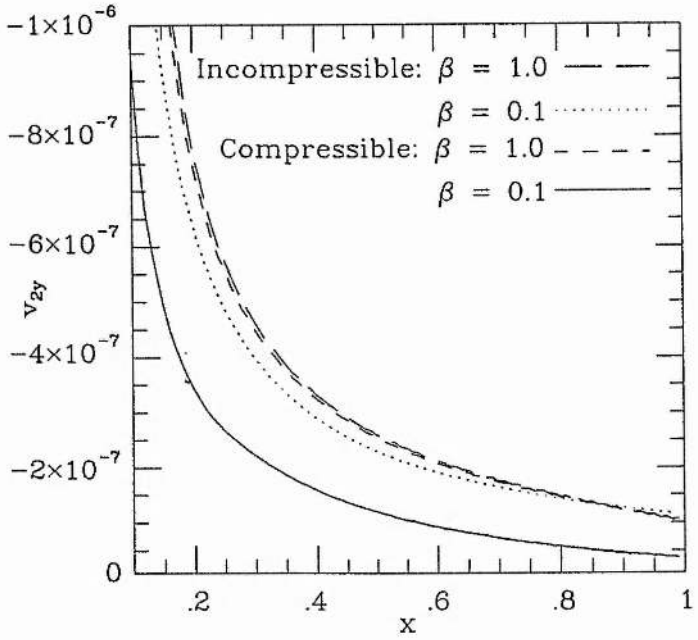

Figure 5.4: The lowest-order y-component of velocity vs. x.

true of the second-order shock position, y_2, which from (5.38) is largest where v_{2y} is largest.

One aspect of these solutions which has not been discussed at all so far is their variation with the plasma beta. Roughly speaking, in a low-beta plasma it is the magnetic field which will provide the dominant force acting on the plasma, whereas in a high-beta plasma, it is the plasma pressure which is dominant. As explained in the introduction, a high-beta plasma will behave incompressibly. Thus, as shown in Figures 5.2, 5.3 and 5.4, increasing β_e has the same effect as increasing γ. Because we have used a perturbation expansion and have assumed that β is order one, we cannot show results for large β. We would expect, however, that as β is increased for both the compressible and incompressible cases, the values of velocity, magnetic field strength, etc would become the same for both.

We find also that the reconnection rate varies with β_e, through the dependence of a_n in (5.3) on R_0. The effect is again similar to increasing γ, i.e. increasing β_e decreases the maximum reconnection rate for regimes with an upstream compression ($b_0 < 1$) and decreases the maximum value of M_i for regimes with an upstream expansion ($b_0 > 1$)

5.6 Summary

We have investigated the effects of including compressibility in models of magnetic reconnection. Comparing these results with the incompressible models of Chapters 1 and 2 (see

also Priest & Forbes, 1986 and Jardine & Priest, 1988a) shows that compressibility modifies the reconnection process quantitatively, without changing its character. The overall behaviour of the solutions is in fact very similar to that found in the incompressible limit and shows the same variations on going from one reconnection regime to the next.

The main modifications are to the way that the reconnection rate varies with the imposed boundary conditions (which determine the reconnection regime) and to the way that the magnetic field influences the flow. For a fully compressible plasma we find that, in cases where there is a compression in the inflow region, the maximum reconnection rate is increased, whereas in cases where there is an expansion in the inflow region, the maximum value of M_i is increased.

The actual form of the solution which is obtained for any given inflow boundary conditions is also changed. In the inflow region the flow is made more strongly converging or diverging by the inclusion of compressibility. In the outflow region, the field lines are curved, as in the incompressible case, but here, since the tension force can compress as well as propel the plasma, the field lines straighten out rather more quickly and there is a correspondingly greater acceleration of the plasma close to the diffusion region. As might be expected, the density, which is uniform in the incompressible case, increases with distance from the diffusion region.

These models have also allowed us to investigate more fully how varying the plasma beta can affect magnetic reconnection. In the compressible case, increasing β tends, in the upstream region, to reduce the convergence or divergence of the flow and, in the downstream region, to decrease v_{1x}, increase B_{1x} and increase the magnitude of v_{2y}. The reconnection rate is also affected, such that increasing β tends to decrease M_e for regimes with $b_0 < 1$ and to decrease M_i for regimes with $b_0 > 1$. As β is increased these changes become less, until, once β is sufficiently large, there are no further variations. Thus, in the incompressible case, none of the above parameters varies with β and only B_e and p_e, the lowest-order upstream magnetic field and pressure are affected.

CHAPTER 6

GLOBAL ENERGETICS OF COMPRESSIBLE RECONNECTION

6.1 Introduction

In Chapter 5 we examined the effects of compressibility on our coupled reconnection models. These effects will, however, also be manifest in the energetics, since in a compressible plasma, the internal energy of the plasma can change. In this chapter, then, we explore the energetics of the compressible solutions and compare our results with those for the incompressible case.

6.2 Global energetics

In a compressible, steady-state plasma, conservation of energy may be expressed by Equation (1.6), i.e.

$$\nabla . \left[(\frac{\gamma}{\gamma - 1} p + \tfrac{1}{2} \rho v^2) \boldsymbol{v} + \frac{\boldsymbol{E} \times \boldsymbol{B}}{\mu} \right] = 0,$$

Integrating this over a volume and using Gauss' theorem gives, in the two-dimensional case,

$$\int_B^C \left[(\frac{\gamma}{\gamma - 1} p + \tfrac{1}{2} \rho v^2) v_y + \frac{E B_x}{\mu} \right] dx + \int_D^C \left[(\frac{\gamma}{\gamma - 1} p + \tfrac{1}{2} \rho v^2) v_x - \frac{E B_y}{\mu} \right] dy = 0, \quad (6.1)$$

As in the incompressible case, this simply states that the amount of energy flowing into a region is equal to that flowing out. Within each set of square brackets the first term represents the thermal energy, the second the kinetic energy and the third the magnetic energy. Both the nondimensionalisation and the expansion of (6.1) are carried out in the same way as in the incompressible case.

To lowest order in this expansion, (6.1) has a very simple form. In the upstream region it reduces to

$$\frac{v_e B_e^2}{2\mu} \left\{ \left[\left(\tfrac{\gamma \beta_e}{\gamma - 1} \right)_{\rm th} + (2)_{\rm mag} \right] - \left[\left(\tfrac{\gamma \beta_e}{\gamma - 1} \right)_{\rm th} + (2)_{\rm mag} \right] \right\} = 0, \quad (6.2)$$

where the first set of terms in square brackets represents the energy flowing in through the top boundary (BC in Figure 4.1) and the second set represents the energy flowing out through the shock. In the downstream region, this becomes

$$\frac{v_e B_e^2}{2\mu}\left\{\left[\left(\frac{\gamma\beta_e}{\gamma-1}+1\right)_{\rm th}+(1)_{\rm kin}\right]-\left[\left(\frac{\gamma\beta_e}{\gamma-1}+1\right)_{\rm th}+(1)_{\rm kin}\right]\right\}=0 \qquad (6.3)$$

where the first set of terms in square brackets represents the energy flowing into the region through the shock and the second set represents the energy flowing out of the side. To this order, then, there is no energy conversion at all within either the upstream or the downstream regions; it is only at the shock that energy is converted. Here, (6.1) becomes

$$\frac{v_e B_e^2}{2\mu}\left\{\left[\left(\frac{\gamma\beta_e}{\gamma-1}\right)_{\rm th}+(2)_{\rm mag}\right]-\left[\left(\frac{\gamma\beta_e}{\gamma-1}+1\right)_{\rm th}+(1)_{\rm kin}\right]\right\}=0 \qquad (6.4)$$

such that, at the shock all the magnetic energy is destroyed and divided equally into the thermal and kinetic contributions. Thus to this order the energy conversion depends only on M_e (through the $v_e B_e^2/2\mu$ term) such that increasing M_e, or the rate at which plasma flows into the upstream region, increases the amount of energy that is converted. Within both the upstream and downstream regions the *total* energy depends on M_e, γ and β_e, but the *ratios* of thermal to magnetic (or kinetic) energy depend only on γ and β_e. Increasing γ decreases the thermal contribution, while increasing β_e increases it. In the limit $\gamma \to \infty$ we recover the incompressible results of Chapter 4 and of Jardine & Priest (1988b) .

At the next order the situation is rather more complex. Within the upstream region we find that there is no energy flow through the top boundary (BC) but energy flows through the side and shock boundaries as

$$\frac{v_e B_e^2}{2\mu}\sum_{n=0}^{\infty} a_n \sinh(n+\tfrac{1}{2})\pi\left\{\left[\frac{\gamma\beta_e}{\gamma-1}\left(\frac{\sin(n+\frac{1}{2})\pi}{(n+\frac{1}{2})\pi}-b_0\left(1+\frac{2}{\gamma\beta_e}\right)\right)_{\rm th}-\left(2\frac{\sin(n+\frac{1}{2})\pi}{(n+\frac{1}{2})\pi}\right)_{\rm mag}\right]\right.$$
$$\left.-\left[\frac{\gamma\beta_e}{\gamma-1}\left(\frac{\sin(n+\frac{1}{2})\pi}{(n+\frac{1}{2})\pi}-b_0\left(1+\frac{2}{\beta_e}\right)\right)_{\rm th}+2\left(b_0-\frac{\sin(n+\frac{1}{2})\pi}{(n+\frac{1}{2})\pi}\right)_{\rm mag}\right]\right\}=0 \qquad (6.5)$$

where the same convention applies to the square brackets. This shows that within the upstream region there is a transfer of energy between the magnetic and thermal components such that the thermal energy increases if $b_0 < 0$, whereas the magnetic energy increases if $b_0 > 0$. This corresponds to the fact that in regimes with $b_0 < 0$ there is a compression in the upstream region with a converging flow which carries thermal energy in through the side boundary. The opposite is true where $b_0 > 0$: here there is an expansion upstream with a diverging flow which carries thermal energy out of the region. Because the system is in a steady state, an increase in the thermal energy must correspond to a decrease in

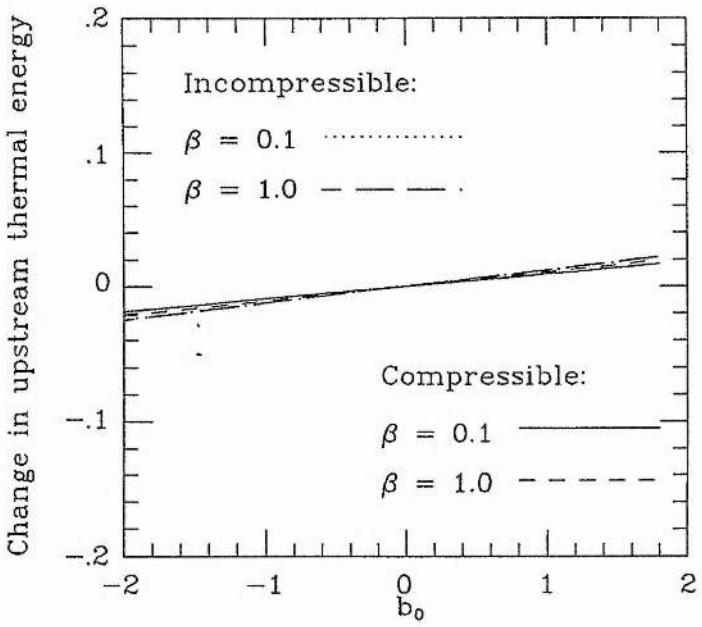

Figure 6.1: The change of thermal energy with b_0 in the upstream region.

the magnetic energy and vice versa. Thus, to this order, the energy conversion depends only on γ or β_e through the κ term in (5.3). Increasing either of these simply increases κ, rescaling the amount of energy converted without changing the nature of its variation with the reconnection regime (see Figure 6.1). We note that a *negative* energy change denotes a net *outflow* of energy and hence an *increase* of energy within the region.

The effects of compressibility become much more pronounced when looking at the energy conversion at the shock. At second order, the energy flow into and out of the shock is described by

$$\begin{aligned}
&\frac{v_e B_e^2}{2\mu}\sum_{n=0}^{\infty} a_n \sinh(n+\tfrac{1}{2})\pi \\
&\quad\times\Bigg\{\Bigg[\left(-\left(\tfrac{\gamma(\beta_e+1)}{\gamma-1}+\tfrac{\gamma}{\gamma-1}\right)b_0+\tfrac{\gamma\beta_e}{\gamma-1}\frac{\sin(n+\frac{1}{2})\pi}{(n+\frac{1}{2})\pi}\right)_{\rm th}+2\left(b_0-\frac{\sin(n+\frac{1}{2})\pi}{(n+\frac{1}{2})\pi}\right)_{\rm mag}\Bigg] \\
&\quad-\Bigg[\left(\left(-\tfrac{\gamma(\beta_e+1)}{\gamma-1}+\tfrac{1}{\gamma-1}\right)b_0+\tfrac{\gamma(\beta_e-1)}{R_0(\gamma-1)}\frac{\sin(n+\frac{1}{2})\pi}{(n+\frac{1}{2})\pi}+\frac{\int_0^1 R_1(x)\,dx}{R_0(1-R_0)(\gamma-1)}\right)_{\rm th} \\
&\quad+\left(\left(\tfrac{\gamma-3}{\gamma-1}-\tfrac{4R_0}{(\gamma-1)(1-R_0)}\right)b_0-\left(\tfrac{4\gamma\beta_e}{\gamma-1}-\tfrac{2\gamma}{R_0(\gamma-1)}+3\right)\frac{\sin(n+\frac{1}{2})\pi}{(n+\frac{1}{2})\pi}-\frac{(1+R_0)\int_0^1 R_1(x)\,dx}{R_0(\gamma-1)(1-R_0)^2}\right)_{\rm kin} \\
&\quad+\left(\tfrac{4R_0}{(\gamma-1)(1-R_0)}b_0+\tfrac{4\gamma\beta_e}{\gamma-1}\frac{\sin(n+\frac{1}{2})\pi}{(n+\frac{1}{2})\pi}+\frac{2\int_0^1 R_1(x)\,dx}{(\gamma-1)(1-R_0)^2}\right)_{\rm mag}\Bigg]\Bigg\}=0 \qquad (6.6)
\end{aligned}$$

where again the first set of terms in square brackets refers to the energy flow into the shock, the second set to the energy flow out of the shock.

At this order the energy conversion depends crucially not only on b_0 but also on γ and β_e. This is hardly surprising, since the very nature of the shock depends on its strength, R, which is itself a function of these variables. Figure (6.2) shows how, to this order, the variation with b_0 of the amount of energy converted changes as γ or β_e is altered. In all cases, as b_0 is increased from the upstream compression regimes ($b_0 < 0$) to the expansions ($b_0 > 0$), the kinetic and thermal energies produced at the shock decrease, while the magnetic energy produced increases. As β is increased, these variations become more pronounced. When β is small, these variations are greater in the compressible case, but as β is increased and the plasma begins to behave incompressibly, the results for both the compressible and incompressible cases become the same.

Within the downstream region, the energy conversion is rather simpler. Expressing the energy flow in through the shock and out through the side, respectively, as

$$\begin{aligned}
&\frac{v_e B_e^2}{2\mu}\sum_{n=0}^{\infty} a_n \sinh(n+\tfrac{1}{2})\pi \left\{ \left[\left(\left(-\frac{\gamma(\beta_e+1)}{\gamma-1}+\frac{1}{\gamma-1}\right) b_0 + \frac{\gamma(\beta_e-1)}{R_0(\gamma-1)}\frac{\sin(n+\frac{1}{2})\pi}{(n+\frac{1}{2})\pi} + \frac{\int_0^1 R_1(x)\,dx}{R_0(1-R_0)(\gamma-1)} \right)_{\text{th}} \right.\right. \\
&\quad + \left(\left(\frac{\gamma-3}{\gamma-1}+\frac{4\gamma(\beta_e+1)}{(\gamma-1)}\right) b_0 - \left(\frac{4\gamma\beta_e}{\gamma-1}-\frac{2\gamma}{R_0(\gamma-1)}+3\right)\frac{\sin(n+\frac{1}{2})\pi}{(n+\frac{1}{2})\pi} - \frac{(1+R_0)\int_0^1 R_1(x)\,dx}{R_0(\gamma-1)(1-R_0)^2} \right)_{\text{kin}} \\
&\quad \left. + \left(-\frac{4\gamma(\beta_e+1)}{(\gamma-1)} b_0 + \frac{4\gamma\beta_e}{\gamma-1}\frac{\sin(n+\frac{1}{2})\pi}{(n+\frac{1}{2})\pi} + \frac{2\int_0^1 R_1(x)\,dx}{(\gamma-1)(1-R_0)^2} \right)_{\text{mag}} \right] \\
&\quad - \left[\left(\left(-\frac{\gamma(\beta_e+1)}{\gamma-1}+\frac{1}{\gamma-1}\right) b_0 + \left(\frac{\gamma\beta_e}{R_0(\gamma-1)}+\frac{(\gamma-2)}{R_0(\gamma-1)}\right)\frac{\sin(n+\frac{1}{2})\pi}{(n+\frac{1}{2})\pi} + \frac{\int_0^1 R_1(x)\,dx}{R_0(1-R_0)(\gamma-1)} \right)_{\text{th}} \right. \\
&\quad \left.\left. + \left(\frac{(\gamma-3)}{(\gamma-1)} b_0 + \left(\frac{2}{R_0(\gamma-1)}+3\right)\frac{\sin(n+\frac{1}{2})\pi}{(n+\frac{1}{2})\pi} + \frac{\int_0^1 R_1(x)\,dx}{R_0(1-R_0)(\gamma-1)} \right)_{\text{kin}} \right] \right\} = 0, \qquad (6.7)
\end{aligned}$$

it can be seen that the thermal energy will increase if $\gamma > 1$ (which is always satisfied) while all of the magnetic energy is simply absorbed into the kinetic energy.

Once again, including compressibility has a noticeable effect on the energy conversion. This essentially comes about because the downstream solution is determined by the boundary conditions at the shock, which are themselves determined by the values of γ and β_e. Thus as shown in Figure 6.3, increasing β_e tends to increase variations with b_0. When β_e is small, these variations are greater in the compressible case. The change with b_0 of the magnetic energy converted is just a mirror image of Figure 6.3, since there is no change in the thermal energy converted with b_0.

Figure 6.4 shows the ratio of the *total* flux of thermal to kinetic energy flowing out of the downstream side boundary. As might be expected, increasing β_e increases this ratio (since more of the energy goes into the thermal component). When β_e is small, this ratio is greater in the compressible case.As noted above, however, once β_e is large enough, there

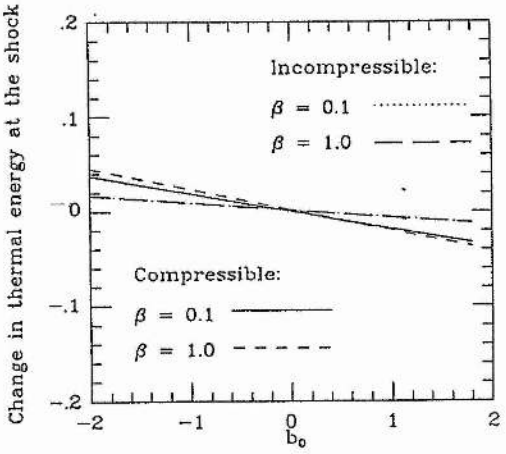

(a)

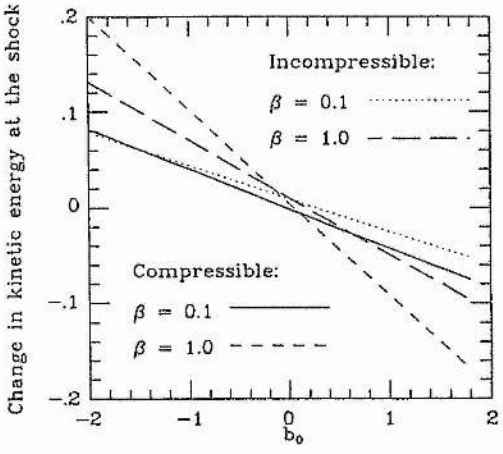

(b)

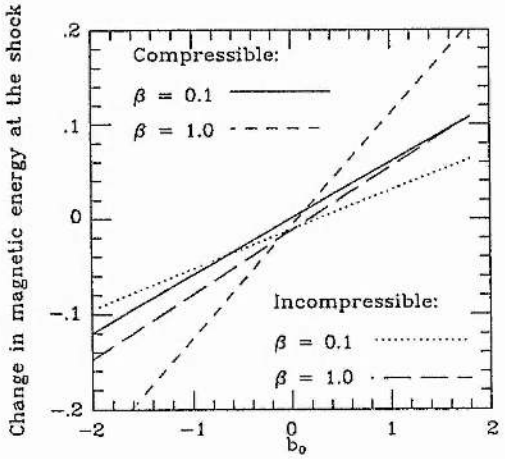

(c)

Figure 6.2: Changes in (a) thermal; (b) kinetic and (c) magnetic energy at the shock.

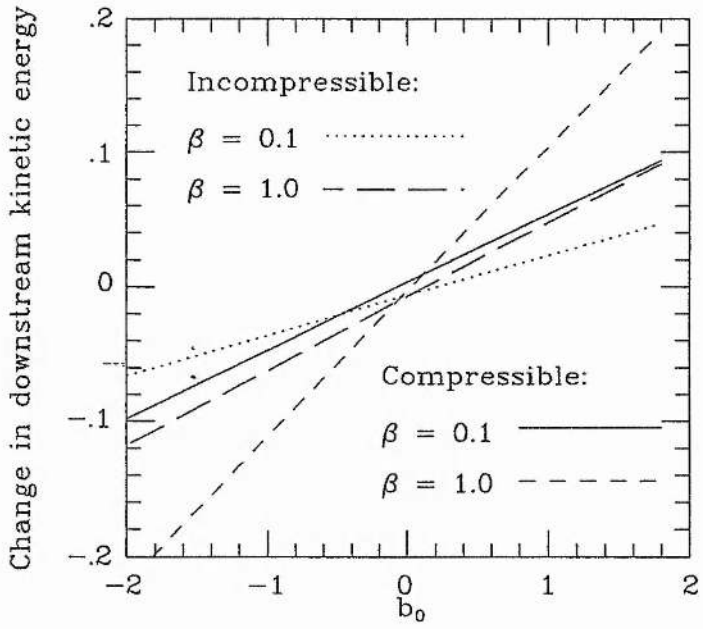

Figure 6.3: The change of kinetic energy with b_0 in the downstream region.

are no longer any density variations and hence no variations in the internal energy. At this stage, the results for the compressible and the incompressible cases should be the same (this limit is not shown because, within the limitations of our expansion, β_e must be of order one). From (6.7) it can also be seen that the gradients of these lines will also depend on whether $\gamma < 3$ or $\gamma > 3$. Thus, if $\gamma > 3$, the ratio of thermal to kinetic energy flowing out of the downstream region decreases with b_0, while if $\gamma < 3$, this ratio increases with b_0.

6.3 Summary

Using as a basis the incompressible results of Chapters 1, 2 and 4 (see also Jardine & Priest (1988c)) we have examined the effects of including compressibility on the global energetics of the reconnection process. To lowest order, where all the energy conversion occurs at the slow shocks we find that there is no change in the amount of energy converted, although the total energy content of the regions upstream and downstream of the shocks is increased.

At the next order, there is a slight increase in the energy conversion in the upstream region, but the effect is much more apparent in the downstream region and at the shocks. Here, allowing compressibility increases the variations in the energy conversion with the reconnection regime. Thus, for a slow compression regime, the magnetic energy increases

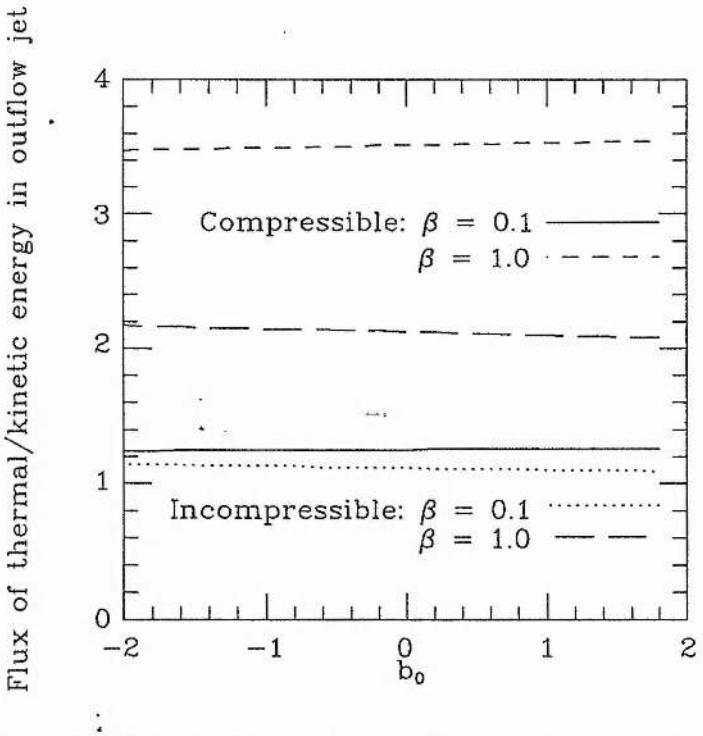

Figure 6.4: The ratio of the total flux of thermal to kinetic energy in the outflow jet.

at the shocks, while the thermal and kinetic energies decrease. For the flux pile-up regime the opposite is true. Within the downstream region, all of the magnetic energy is absorbed into the kinetic energy, while the thermal energy increases at the expense of the kinetic energy. Again, the amount of energy converted is increased by allowing compressibility.

The ratio of the total thermal and kinetic energies flowing out of the downstream region is also affected: in a compressible plasma this ratio is higher and increases on going from a slow compression regime to a flux pile-up regime, while in an incompressible plasma, this ratio is lower and decreases with this change in regime.

Finally, allowing for compressibility has enabled us to examine fully the effects of varying the plasma beta. As can be seen most clearly at lowest order, one result of increasing β_e is to increase the thermal contribution to the total energy. At higher orders, we find also that this increases the variations in the energy conversion with b_0. When β is small, these variations are greater for the compressible case, but as β is increased and the plasma becomes incompressible, the results for the compressible and incompressible plasmas will become the same.

APPENDIX A

THE DOWNSTREAM SOLUTION

From (2.12) it can be seen that the characteristics of the solution for B_{1x} lie along the lines $y = \pm M_e x + c$. Hence these will divide the downstream region into three parts, depending on whether the characteristics emanate from the diffusion region or the wave (see Figure A.1). Region 1 is crossed only by characteristics from the diffusion region; region 2 by characteristics from the diffusion region and the waves and region 3 by characteristics from the waves only. Since these characteristics define the directions along which information from the boundaries propagates into the solution, the lines $y = \pm(M_e x - 2M_e L)$ define the separate regions of influence of the boundary conditions.

Clearly, if we wish to select solutions for which the diffusion region has least effect on the downstream region, we need $L \ll 1$, such that regions 1 and 2 are small enough to be neglected. In this case, however, it is not clear what is the correct boundary condition to use for region 3, which does not extend to the wave. To clarify this point, we consider all three regions:

Region 1

The boundary conditions are

1. $B_{1x} = 0$ on $y = 0$,
2. $B_{1x} = h(y)$ on $x = L$ (where h is an odd function of y),
3. $\frac{\partial B_{1x}}{\partial x} = 0$ on $x = L$.

We therefore obtain from (2.12)

$$B_{1x}(x, y) = \tfrac{1}{2}h(y - M_e x + M_e L) + \tfrac{1}{2}h(y + M_e x - M_e L). \qquad \text{(A.1)}$$

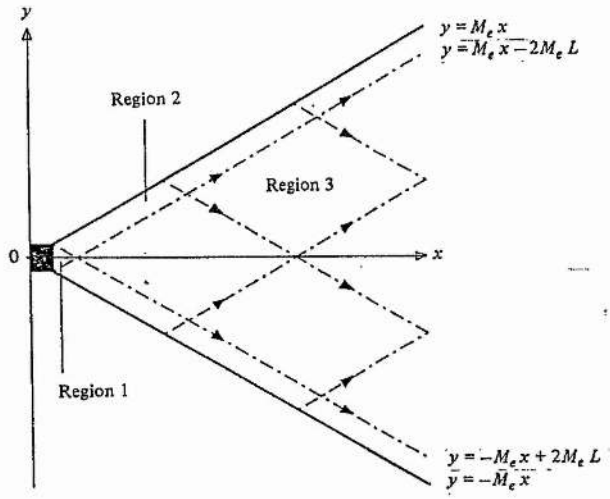

Figure A.1: Characteristics for the solution for B_{1x} in the downstream region.

Region 2

Here the boundary conditions are

1. $B_{1x} = h(y)$ on $x = L$,

2. $B_{1x} = B_{1x}^d(x)$ on $y = M_e x$ (where B_{1x}^d is given by the jump relations).

Since the $y = M_e x + c$ characteristics are common to regions 1 and 2, (2.12) gives

$$B_{1x}(x,y) = \tfrac{1}{2}h(y - M_e x + M_e L) + B_{1x}^d\left[\frac{1}{2M_e}(y + M_e x)\right] - \tfrac{1}{2}B_{1x}^d(L). \qquad \text{(A.2)}$$

Region 3

Here the boundary conditions are

1. $B_{1x} = 0$ on $y = 0$,

2. $B_{1x} = B_{1x}^d(x)$ on $y = M_e x$

and noting that the $y = -M_e x + c$ characteristics will be common to regions 2 and 3, we obtain, from (2.12),

$$B_{1x}(x,y) = B_{1x}^d\left[\frac{1}{2M_e}(y + M_e x)\right] - B_{1x}^d\left[\frac{1}{2M_e}(y - M_e x)\right]. \qquad \text{(A.3)}$$

Now, the corresponding velocities can be found by substituting (A.1)–(A.3) into (2.6) and the y-derivative of (2.7), i.e.

$$\frac{\partial v_{1x}}{\partial x} = -\frac{1}{\rho v_{Ae}}\frac{dp_1}{dx} + \frac{M_e}{(\mu\rho)^{1/2}}\frac{\partial B_{1x}}{\partial x} \tag{A.4}$$

$$\frac{\partial v_{1x}}{\partial y} = \frac{1}{M_e(\mu\rho)^{1/2}}\frac{\partial B_{1x}}{\partial x}. \tag{A.5}$$

Integrating these and using for regions 1 and 2 the condition that $v_{1x} = v_{1x}^d$ on $y = M_e x$ gives

$$\begin{aligned} v_{1x}(x,y) &= v_{1x}^d - \frac{1}{2(\mu\rho)^{1/2}}[h(y - M_e x + M_e L) - h(y + M_e x - M_e L) \\ &\quad -h(M_e L) - h(-2M_e x + M_e L)] \text{ in region 1;} \end{aligned} \tag{A.6}$$

$$\begin{aligned} v_{1x}(x,y) &= v_{1x}^d + \frac{1}{(\mu\rho)^{1/2}}\left\{B_{1x}^d\left[\frac{1}{2M_e}(y + M_e x)\right] - B_{1x}^d \right. \\ &\quad \left. +\tfrac{1}{2}B_{1x}^d(L) - \tfrac{1}{2}h[y - M_e x + M_e L]\right\} \text{ in region 2.} \end{aligned} \tag{A.7}$$

For region 3 we use the condition that at the boundary between regions 2 and 3 the velocities obtained in the two regions must be the same, i.e. the velocity obtained from (2.6) and (2.7)

$$v_{1x} = c - \frac{p_1}{\rho v_{Ae}} + \frac{1}{(\mu\rho)^{1/2}}\left\{B_{1x}^d\left[\frac{1}{2M_e}(y + M_e x)\right] + B_{1x}^d\left[\frac{1}{2M_e}(y - M_e x)\right]\right\} \tag{A.8}$$

must be equal to that from (A.7). Evaluating (A.7) and (A.8) at $y = M_e x - 2M_e L$ and solving gives

$$c - \frac{p_1}{\rho v_{Ae}} = v_{1x}^d - \frac{B_{1x}^d}{(\mu\rho)^{1/2}} \text{ (with } c \text{ a constant),} \tag{A.9}$$

and hence

$$v_{1x}(x,y) = v_{1x}^d + \frac{1}{(\mu\rho)^{1/2}}\left\{B_{1x}^d\left[\frac{1}{2M_e}(y + M_e x)\right] + B_{1x}^d\left[\frac{1}{2M_e}(y - M_e x)\right] - B_{1x}^d(x)\right\}, \tag{A.10}$$

or, using the jump relation for B_{1x}^d (2.29), we have

$$B_{1x}(x,y) = B_{1x}^u\left[\frac{1}{2M_e}(y + M_e x)\right] + B_{1x}^u\left[\frac{1}{2M_e}(y - M_e x)\right], \tag{A.11}$$

$$v_{1x}(x,y) = \frac{1}{(\mu\rho)^{1/2}}\left\{B_{1x}^u\left[\frac{1}{2M_e}(y + M_e x)\right] + B_{1x}^u\left[\frac{1}{2M_e}(y - M_e x)\right] - B_{1x}^u(x)\right\} \text{ for region 3.} \tag{A.12}$$

Hence in the downstream region if $L \ll 1$ then (A.11) and (A.12) will be valid over most of the downstream region. Both v_{1x} and B_{1x} are specified completely by the upstream solution, and the choice of v_{1x}^d only influences the narrow region close to the wave. In fact, if the diffusion region is very small then at $x = L$, $B_{1x}^d \approx 0$ (since by symmetry it must be

zero on the x-axis). In this case, from (2.29), $v_{1x}^d \approx B_{1x}^u(L)/(\mu\rho)^{1/2}$. In general we expect jets of plasma in the regions close to the wave (Soward & Priest 1986), but their effect will be negligible when L is small enough.

APPENDIX B

THE JUMP RELATIONS

We may express the velocity and magnetic field vectors in components normal to and transverse to the wave as follows:

$$\begin{aligned}
v^u &= [-v^u \cos[\tfrac{1}{2}\pi - (\Phi - \alpha)], v^u \sin[\tfrac{1}{2}\pi - (\Phi - \alpha)]], \\
b^u &= [B^u \cos[\tfrac{1}{2}\pi - (\Omega - \alpha)], -B^u \sin[\tfrac{1}{2}\pi - (\Omega - \alpha)]], \\
v^d &= [-v^d \cos[\tfrac{1}{2}\pi - (M + \alpha)], -v^d \sin[\tfrac{1}{2}\pi - (M + \alpha)]], \\
b^d &= [B^d \cos[\tfrac{1}{2}\pi - (L - \alpha)], -B^d \sin[\tfrac{1}{2}\pi - (L - \alpha)]],
\end{aligned}$$

where Φ, Ω, etc. are defined in Figure 2.1.

Writing the jump relations (2.21) in terms of these angles, we have

$$v^u \cos[\tfrac{1}{2}\pi - (\Phi - \alpha)] = v_A^u \cos[\tfrac{1}{2}\pi - (\Omega - \alpha)], \tag{B.1}$$

$$v^u \cos[\tfrac{1}{2}\pi - (\Phi - \alpha)] = v^d \cos[\tfrac{1}{2}\pi - (M + \alpha)], \tag{B.2}$$

$$\begin{aligned}
v^u \sin[\tfrac{1}{2}\pi - (\Phi - \alpha)] + v^d \cos[\tfrac{1}{2}\pi - (M + \alpha)] \\
= -\frac{1}{(\mu\rho)^{1/2}} \Big\{ -B^u \sin[\tfrac{1}{2}\pi - (\Omega - \alpha)] \\
+ B^d \sin[\tfrac{1}{2}\pi - (\Omega - \alpha)] \Big\},
\end{aligned} \tag{B.3}$$

$$B^u \cos[\tfrac{1}{2}\pi - (\Omega - \alpha)] = B^d \cos[\tfrac{1}{2}\pi - (L - \alpha)] \tag{B.4}$$

$$p^d = p^u + \frac{1}{2\mu}[(B^u)^2 - (B^d)^2] \tag{B.5}$$

where

$$\left.\begin{aligned}
v^u \sin\Phi &= -v_y^u, \quad v^d \sin M = -v_y^d, \\
v^u \cos\Phi &= -v_x^u, \quad v^d \cos M = v_x^d. \\
B^u \sin\Omega &= B_y^u, \quad B^d \cos L = B_x^d, \\
B^u \cos\Omega &= B_x^u, \quad B^d \sin L = B_y^d.
\end{aligned}\right\} \tag{B.6}$$

Equations (B.1) - (B.6) may now be written in terms of the $x-$ and $y-$ components given in (B.6) and the resulting equations expanded in powers of M_e, assuming the following ordering:

upstream

$$\begin{aligned}
v_x &= && && \epsilon^2 v_{2x} &+\cdots \\
v_y &= && \epsilon v_{1y} &+ \epsilon^2 v_{2y} &+\cdots \\
B_x &= B_{0x} &+ \epsilon B_{1x} &+ \epsilon^2 B_{2x} &+\cdots \\
B_y &= && \epsilon B_{1y} &+ \epsilon^2 B_{2y} &+\cdots \\
p &= p_0 &+ \epsilon p_1 &+ \epsilon^2 p_2 &+\cdots;
\end{aligned}$$

downstream

$$\begin{aligned}
v_x &= v_{0x} &+ \epsilon v_{1x} &+ \epsilon^2 v_{2x} &+\cdots \\
v_y &= v_{0y} &+ \epsilon v_{1y} &+ \epsilon^2 v_{2y} &+\cdots \\
B_x &= B_{0x} &+ \epsilon B_{1x} &+ \epsilon^2 B_{2x} &+\cdots \\
B_y &= B_{0y} &+ \epsilon B_{1y} &+ \epsilon^2 B_{2y} &+\cdots \\
p &= p_0 &+ \epsilon p_1 &+ \epsilon^2 p_2 &+\cdots.
\end{aligned}$$

The resulting equations are

$$\left.\begin{aligned}
O(1) \quad \tan\alpha_0 &= 0, \\
O(\epsilon) \quad \tan\alpha_1 &= \tfrac{B^u_{1y}}{B_e} + \tfrac{v_e}{v_{Ae}}, \\
O(\epsilon^2) \quad \tan\alpha_1 &= \tfrac{B^u_{2y}}{B_e} - \tfrac{B^u_{1x}}{B_e}\tan\alpha_1 - \tfrac{v_e}{v_{Ae}}\tfrac{B^u_{1x}}{B_e};
\end{aligned}\right\} \tag{B.7}$$

$$\left.\begin{aligned}
O(1) \quad v_{0y} &= 0, \\
O(\epsilon) \quad \pm v_{1y} &= -v^u_{1y} - v^d_{0x}\tan\alpha_1, \\
O(\epsilon^2) \quad \pm v_{2y} &= -v^d_{0x}\tan\alpha_2 - v^d_{1x}\tan\alpha_1 - v^u_{2y};
\end{aligned}\right\} \tag{B.8}$$

$$\left.\begin{aligned}
O(1) \quad \pm B^d_{0y} &= 0, \\
O(\epsilon) \quad \pm B^d_{1y} &= B^u_{1y} - B^u_{0x}\tan\alpha_1 + B^d_{0x}\tan\alpha_1, \\
O(\epsilon^2) \quad \pm B^d_{2y} &= B^u_{2y} - B^u_{0x}\tan\alpha_2 - B^u_{1x}\tan\alpha_1 + B^d_{0x}\tan\alpha_2 + B^d_{1x}\tan\alpha_1;
\end{aligned}\right\} \tag{B.9}$$

$$\left.\begin{aligned}
O(1) \quad p^d_0 &= p^u_0 + \tfrac{1}{2\mu}[(B^u_{0x})^2 - (B^d_{0x})^2], \\
O(\epsilon) \quad p^d_1 &= p^u_1 + \tfrac{B^u_{0x}}{\mu}B^u_{1x} - \tfrac{B^d_{0x}}{\mu}B^d_{1x}, \\
O(\epsilon^2) \quad p^d_2 &= p^u_2 + \tfrac{1}{2\mu}[2B^u_{0x}B^u_{2x} - 2B^d_{0x}B^d_{2x} + (B^u_{1x})^2 + (B^u_{1y})^2 - (B^d_{1x})^2 - (B^d_{1y})^2];
\end{aligned}\right\} \tag{B.10}$$

where the $\pm$ signs correspond to the signs of v_y and B_x (see Fig. 2.1). Introducing the assumption that $v_{0x} = v_{Ae}$ (and the corresponding result that $v^d_{1y} = 0$) now gives (2.22) to (2.36).

APPENDIX C

THE DOWNSTREAM MAGNETIC FIELD

The equation which governs the perturbed x-component of the downstream magnetic field $B_{1x}(x,y)$ is

$$\overline{B}_{1x}(x,y) = f(y - \frac{M_e}{R_0^{1/2}}x) + g(y + \frac{M_e}{R_0^{1/2}}x) \tag{C.1}$$

where f and g are arbitrary functions. The boundary conditions

$$1.\ \overline{B}_{1x} = 0 \qquad \text{on} \qquad y = 0 \tag{C.2}$$

$$2.\ \overline{B}_{1x} = \overline{B}^d_{1x} \qquad \text{on} \qquad y = M_e x/R_0 \tag{C.3}$$

give

$$-f(-u) = g(u) \tag{C.4}$$

$$\overline{B}^d_{1x}\left[\frac{R_0 u}{M_e(1+R_0^{1/2})}\right] = f(-\xi u) + g(u) \tag{C.5}$$

where

$$\xi = \frac{R_0^{1/2}-1}{R_0^{1/2}+1} < 1.$$

Using (C.4) this is just

$$\begin{aligned} g(u) &= g(\xi u) + \overline{B}^d_{1x}\left[\frac{R_0 u}{M_e(1+R_0^{1/2})}\right] \\ &= g(\xi^Q u) + \sum_{q=0}^{Q} \overline{B}^d_{1x}\left[\xi^q \frac{R_0 u}{M_e(1+R_0^{1/2})}\right]. \end{aligned}$$

Now, as $Q \to \infty$, $\xi^Q \to 0$ since $\xi < 1$. Hence, as $Q \to \infty$,

$$g(u) = g(0) + \sum_{q=0}^{\infty} \overline{B}^d_{1x}\left[\xi^q \frac{R_0 u}{M_e(1+R_0^{1/2})}\right]$$

and hence, using (C.4)

$$f(u) = -g(0) - \sum_{q=0}^{\infty} \overline{B}^d_{1x}\left[\xi^q \frac{R_0 u}{M_e(1+R_0^{1/2})}\right]$$

(since $\overline{B}^d_{1x}$ is an even function). Thus (C.1) becomes

$$\overline{B}_{1x}(x,y) = \sum_{q=0}^{\infty} \overline{B}^d_{1x}(\xi^q c^+) - \overline{B}^d_{1x}(\xi^q c^-) \tag{C.6}$$

where

$$c^+ = \frac{R_0}{M_e(1+R_0^{1/2})}(y + \frac{M_e}{R_0^{1/2}}x)$$

and

$$c^- = \frac{R_0}{M_e(1+R_0^{1/2})}(y - \frac{M_e}{R_0^{1/2}}x).$$

Now, from (5.46) and (5.44), using (C.6)

$$\overline{v}_{1x}(x,y) = h(x) + \frac{1}{R_0^{1/2}} \sum_{q=0}^{\infty} \overline{B}^d_{1x}(\xi^q c^+) + \overline{B}^d_{1x}(\xi^q c^-) \tag{C.7}$$

and

$$\overline{v}_{1x}(x,y) = t(y) - \frac{\beta_e}{2R_0}\overline{p}^d_1 + \frac{1}{R_0^{1/2}} \sum_{q=0}^{\infty} \overline{B}^d_{1x}(\xi^q c^+) + \overline{B}^d_{1x}(\xi^q c^-) \tag{C.8}$$

where h(x) and t(y) are arbitrary functions. Eliminating $\overline{v}_{1x}$ from (C.7) and (C.8) gives

$$h(x) + \frac{\beta_e}{2R_0}\overline{p}^d_1 = t(y) = a_1, \text{ a constant.} \tag{C.9}$$

Using this and evaluating (C.8) at the shock ($y = M_e x/R_0$) gives

$$\begin{aligned} \overline{v}^d_{1x} &= a_1 - \frac{\beta_e}{2R_0}\overline{p}^d_1(x) + \frac{1}{R_0^{1/2}} \sum_{q=0}^{\infty} \overline{B}^d_{1x}(\xi^q x) + \overline{B}^d_{1x}(\xi^{q+1}x) \\ &= a_1 - \frac{\beta_e}{2R_0}\overline{p}^d_1(x) + \frac{\overline{B}^d_{1x}}{R_0^{1/2}} + \frac{2}{R_0^{1/2}} \sum_{q=0}^{\infty} \overline{B}^d_{1x}(\xi^{q+1}x) \end{aligned}$$

and hence

$$\sum_{q=0}^{\infty} \overline{B}^d_{1x}(\xi^{q+1}x) = \frac{R_0^{1/2}}{2}\left(\overline{v}^d_{1x}(x) + \frac{\beta_e}{2R_0}\overline{p}^d_1(x) - \frac{\overline{B}^d_{1x}(x)}{R_0^{1/2}} - a_1\right). \tag{C.10}$$

This can be substituted into (C.6) to give (5.48) or into (C.8) to give (5.50).

APPENDIX D

THE PERTURBED SHOCK STRENGTH

The equation which determines $R_1(x)$ is (5.52):

$$\begin{aligned}(c_3 - c_2)R_1(x) + (c_3 + c_2)R_1(\xi x) \;=\; & \frac{2\kappa M_e}{L}\sum_{n=0}^{\infty}\frac{\tanh\left[(n+\frac{1}{2})\pi\right]\sin\left[(n+\frac{1}{2})\pi L\right]}{\left[(n+\frac{1}{2})\pi\right]^2} \\ & \times\left\{-(c_0+c_1)\cos\left[(n+\frac{1}{2})\pi x\right]\right. \\ & \left.+(c_0-c_1)\cos\left[(n+\frac{1}{2})\pi\xi x\right] - c_4 b_0\right\}, \qquad \text{(D.1)}\end{aligned}$$

where the constants c_0 to c_4 are as defined in (5.52). Writing the right-hand side, which is a known function, as $f(x)$, we have

$$f(x) = (c_3 - c_2)R_1(x) + (c_3 + c_2)R_1(\xi x) \qquad \text{(D.2)}$$

where we may expand $R_1(x)$ and $R_1(\xi x)$ as a Taylor series about $x = 0$ to give

$$\begin{aligned}f(x) \;=\; & 2c_3R_1(0) \;+\; \tfrac{1}{2!}x^2R_1''(0)\{(c_3-c_2)+\xi^2(c_3+c_2)\} \\ & +\; \tfrac{1}{4!}x^4R_1''''(0)\{(c_3-c_2)+\xi^4(c_3+c_2)\}+\cdots\end{aligned}$$

where all the odd derivatives are zero from (D.1). It can be shown that $(c_3 - c_2) \gg \xi^4(c_3 + c_2)$ and therefore, since $\xi < 1$, $(c_3 - c_2) \gg \xi^6(c_3 + c_2)$ etc. Hence we may neglect the $\xi^n(c_3 + c_2)$ term for $n \geq 4$. This gives

$$f(x) \simeq (c_3 + c_2)R_1(0) + \tfrac{1}{2}x^2R_1''(0)\xi^2(c_3 + c_2) + (c_3 - c_2)R_1(x)$$

and so

$$R_1(x) \simeq \frac{1}{c_3 - c_2}\left\{f(x) - (c_3 + c_2)\left(R_1(0) + \frac{(\xi x)^2}{2}R_1''(0)\right)\right\} \qquad \text{(D.3)}$$

where $f(x)$ is given by (D.1).

$R_1''(0)$ may be found by differentiating $f(x)$ to give

$$\begin{aligned} f'(x) &= \frac{2\kappa M_e}{L}\sum_{n=0}^{\infty}\frac{\tanh\left[(n+\frac{1}{2})\pi\right]\sin\left[(n+\frac{1}{2})\pi L\right]}{(n+\frac{1}{2})\pi} \\ &\quad\times\left\{(c_0+c_1)\sin\left[(n+\tfrac{1}{2})\pi x\right]-\xi(c_0-c_1)\sin\left[(n+\tfrac{1}{2})\pi\xi x\right]\right\}, \\ &\simeq \frac{\kappa M_e}{L}\sum_{n=0}^{\infty}(c_0+c_1)\left\{\frac{\cos[(n+\frac{1}{2})\pi(L-x)]}{np}-\frac{\cos[(n+\frac{1}{2})\pi(L+x)]}{np}\right\} \\ &\quad-\xi(c_0-c_1)\left\{\frac{\cos[(n+\frac{1}{2})\pi(L-\xi x)]}{np}-\frac{\cos[(n+\frac{1}{2})\pi(L+\xi x)]}{np}\right\} \end{aligned}$$

where we have neglected the $\tanh(n+\frac{1}{2})\pi$ term since this tends to one very rapidly. This series may be summed (Gradshteyn & Ryzhik 1980, p. 38) to give

$$f'(x)\simeq\frac{\kappa M_e}{\pi L}\left\{(c_0+c_1)\log\left|\frac{\tan\frac{\pi}{4}(L+x)}{\tan\frac{\pi}{4}(L-x)}\right|-\xi(c_0-c_1)\log\left|\frac{\tan\frac{\pi}{4}(L+\xi x)}{\tan\frac{\pi}{4}(L-\xi x)}\right|\right\}$$

and so

$$f''(0)\simeq\frac{\kappa M_e}{L\sin\frac{\pi L}{2}}\left\{(c_0+c_1)-\xi^2(c_0-c_1)\right\}. \tag{D.4}$$

Now, from (D.1)

$$f''(0)=R_1''(0)\left\{(c_3-c_2)+\xi^2(c_3+c_2)\right\},$$

and so

$$R_1''(0)\simeq\frac{\kappa M_e}{L\sin\frac{\pi L}{2}}\left\{\frac{(c_0+c_1)-\xi^2(c_0-c_1)}{(c_3-c_2)+\xi^2(c_3+c_2)}\right\}. \tag{D.5}$$

Since, also from (D.1),

$$R_1(0)=\frac{f(0)}{2c_3}, \tag{D.6}$$

$R_1(x)$ is now known.

REFERENCES

[1] Asseo, E. & Sol, H., 1986. *Phys. Rep.* , **148**, 308.

[2] Biskamp, D., 1982. *Phys. Lett*, **87A**, 357–360.

[3] Biskamp, D., 1984a. *Phys. Lett*, **105A**, 124–128.

[4] Biskamp, D., 1984b. In Hones, M., editor, *Magnetic Reconnection in Space and Laboratory Plasmas*, pages 369–371, A.G.U., Washington, D.C.

[5] Biskamp, D., 1986. *Phys. Fluids*, **29**, 1520.

[6] Bonnet, R.M. & Dupree, A.K., editors, 1981. *Solar Phenomena in Stars and Stellar Systems*. D. Reidel.

[7] Forbes, T.G., 1982a. *Solar Phys.*, **81**, 303–324.

[8] Forbes, T.G., 1982b. *Planet. Space Sci.*, **30**, 1183–1197.

[9] Forbes, T.G. & Priest, E.R., 1983a. *Solar Phys.*, **84**, 169–188.

[10] Forbes, T.G. & Priest, E.R., 1983b. *J. Geophys. Res.*, **88**, 863–870.

[11] Forbes, T.G. & Priest, E.R., 1987. *Rev. Geophys.* in press.

[12] Fu, Z.F. & Lee, L.C., 1985. *Geophys. Res. Lett.*, **12**, 291–294.

[13] Gradshteyn, I.S. & Ryzhik, I.M., 1980. *Tables of Integrals, Series, and Products*. Academic Press, London, fourth (english translation) edition.

[14] Gratton, F.T., Heyn, M.F., Biernat, H.K., Rijnbeek, R.P., & Gnavi, G., 1988. In *Proc. 21st ESLAB Symposium*, pages 143–148, ESA Spec. Publ. SP-275.

[15] Green, R.M. & Sweet, P.A., 1967. *Astrophys. J.*, **147**, 1153–1156.

[16] Heyn M.F., Biernat, H.K., & Semenov, V.S., 1986. *Adv. Sp. Res.*, **6**, 115–117.

[17] Hones, M., editor, 1984. *Magnetic Reconnection in Space and Laboratory Plasmas*. A.G.U., Washington, D.C.

[18] Jardine. M. & Priest, E.R., 1988a. *J. Plasma Phys.*, **40**, 143–161.

[19] Jardine. M. & Priest. E.R., 1988b. *Geophys. Astrophys. Fluid Dyn.*, **42**, 163–168.

[20] Jardine, M. & Priest, E.R., 1988c. *J. Plasma Phys.* in press.

[21] Jeffrey, A. & Taniuti, T., 1964. *Non-Linear Wave Propagation.* Academic Press.

[22] Kantrowitz, A.R. & Petschek, H.E., 1966. In Kunkel, W.B., editor, *Plasma Physics in Theory and Applications*, McGraw-Hill, New York.

[23] Lee, L.-C. & Fu, Z.F., 1986a. *J. Geophys. Res.*, **91**, 6807–6815.

[24] Lee, L.-C. & Fu, Z.F., 1986b. *J. Geophys. Res.*, **91**, 4551–4556.

[25] Mestel, L., 1985. *Physica Scripta*, **T11**, 53–58.

[26] Parker, E.N., 1963. *Astrophys. J. Suppl.*, **8**, 177–212.

[27] Petschek, H.E., 1964. In *AAS-NASA Symposium on the Physics of Solar Flares*, pages 425–439, NASA Spec. Publ. SP-50.

[28] Petschek, H.E. & Thorne, R.M., 1967. *Astrophys. J.*, **147**, 1157–1163.

[29] Priest, E.R., 1984. *Solar Magnetohydrodynamics.* D. Reidel, Dordrecht.

[30] Priest, E.R., 1985. *Rep. Prog. Phys.* , **48**, 955.

[31] Priest, E.R. & Forbes, T.G., 1986. *J. Geophys. Res.*, **91**, 5579–5588.

[32] Schindler, K. & Birn, J., 1987. *J. Geophys. Res.*, **92**, 95–108.

[33] Semenov, V.S., Kubyshkin, I.V., & Heyn, M.F., 1983. *J. Plasma Phys.*, **30**, 303–320.

[34] Semenov, V.S., Kubyshkin, I.V., Heyn, M.F., & Biernat, H.K., 1983. *J. Plasma Phys.*, **30**, 321–344.

[35] Shivamoggi, B.K., 1985. *Phys. Rep.*, **127**, 99–184.

[36] Sonnerup, B.U.O., 1970. *J. Plasma Phys.*, **4**, 161–174.

[37] Sonnerup, B.U.O., 1979. In Lanzerotti, L.T., Kennel, C.F., & Parker, E.N., editors, *Solar System Plasma Physics*, pages 45–102, North-Holland.

[38] Sonnerup, B.U.O., 1988. *Comp. Phys. Comm.* in press.

[39] Sonnerup, B.U.O & Priest, E.R., 1975. *J. Plasma Phys.*, **14**, 283–284.

[40] Soward, A. & Priest, E.R., 1977. *Phil. Trans. Roy. Soc.* , **A284**, 369.

[41] Soward, A. & Priest, E.R., 1986. *J. Plasma Phys.*, **35**, 333–350.

[42] Sweet, P.A., 1958. In B. Lehnert, editor, *Electromagnetic Phenomena in Cosmical Physics*, pages 124–134, Cambridge University Press.

[43] Ugai, M., 1987. *Phys. Fluids*, **30**, 2163–2166.

[44] Vasyliunas, V.M., 1975. *Rev. Geophys. Space Phys.* , **13**, 303–336.

[45] Yeh, T. & Axford, W.I., 1970. *J. Plasma Phys.*, 4, 207–229.